We thank the reviewers for their thoughtful comments and suggestions. We have addressed all comments. Below is our point-by-point response to the comments of both reviewers, reproduced in black, followed by our response in red.

Response to referee #2

General comments
The authors present a series of observations of turbulent dissipation from measurements taken during two separate research cruises in the region along the slope north of Svalbard. The study considers wind forcing and tides as drivers to mix heat that is concentrated in warm Atlantic-origin water that resides in the mid-depths of the water column. Vertical profiles of turbulent dissipation, diffusivity, and heat and buoyancy fluxes are presented and tied to seasonal changes and input work from both winds and tides. Near the end of the paper, the authors extrapolate their ideas across a broader region. This manuscript makes an important addition to the body of literature on turbulence and mixing in a key Arctic region.

Thanks for these comments! We are happy to read that our study is well-received.

While the results and analysis are interesting and merit publication, the manuscript would be greatly improved by more cohesive linking of the different ideas. As presented, the study reads as a nice collection of related results, but parts of the discussion do more to highlight some of the background and motivation than to link to those results, and many of the results are considered independently despite parallels in the analysis. Consequently, the study lacks a coherent story. There is enough detail in the manuscript already that this should not require any further analysis, but the authors should consider some reorganization of the discussion section to tie together different aspects of the study.

We agree that some reorganization was needed in the discussion to better highlight our results. The changes we made are described below in the point-by-point response to the reviewer. To summarize the main changes: we reordered the result sections (upper layer, tidal forcing and Atlantic water heat loss) for more coherence. We also reorganized the discussion as suggested by both reviewers.

One potential approach to this reorganization would be to rethink the presentation of sections 4-6. Currently, these sections are organized to step vertically down through the water column from the upper ocean (§4) to Atlantic Water (§5), to the bottom boundary layer (§6). However, the wind forcing and tides are presented as the main drivers of vertical mixing while, in some capacity, the Atlantic Water is what is being mixed. It may be better to move some of the ideas from section 5 to the discussion, and use it to unify and compare/contrast the different results from sections 4 and 6 (e.g., is the structure seen in figure 7 a consequence of the results in sections 4 or 6?). Then presenting wind forcing and tidal forcing back-to-back will better highlight the parallels between the analysis in each of those sections.

Thanks for this suggestion. We agree that having both forcing (wind and tide) sections following each other is a better structure, and revised accordingly. We decided to keep the section on the Atlantic Water heat loss as it is, and did not integrate it to the discussion. The material in this part is "results" and is not suitable to introduce in “discussion”. We cannot attribute the structure seen in figure 7 to a consequence of the results in sections 4 and 6.

Specific comments

- L106-107: Here you state that VMP measurements of temperature and salinity agreed with ship CTD profiles, so no corrections were made. But in L129-130 you discuss using the ship CTD to correct the VMP temperature. Please ensure your statements are consistent.

Thanks for pointing this out. No correction was needed, we deleted 'correct' l. 130.

- L116-122: There are a wide number of parameterizations and methods for determining diapycnal diffusivity. You should discuss the sensitivity of your results to the choice of the Bouffard and Boegman (2013) method compared (at least) to the more common Osborn (1980) method with Gamma = 0.2.

The Bouffard and Boegman (2013) method differs from the Osborn (1980) method only for very low and very large Reynolds numbers. In our dataset, 80% of the Reynolds number falls between 8.5 and 400, and for this range of Reynolds number the diapycnal diffusivity is identical in both Bouffard and Boegman (2013) and Osborn (1980). Using Bouffard and Boegman (2013) resulted in fewer outliers, which is why this method was used. Our results are not sensitive to the choice of Bouffard and Boegman (2013) compared to Osborn (1980). We added in the text (after the introduction of Reb):
'In the transitional range (8.5<Reb< 400), calculation of \kappa is identical to Osborn (1980), using the canonical mixing coefficient of 0.2 (Gregg et al. 2018); however in the energetic regime the latter is an overestimate. In our dataset, 80% of the estimates are in the transitional regime.'

- L134: The measurement height for wind speed should be mentioned here, along with the correction to 10m, instead of L248-249.

Agree, we move this explanation l.134.

- L135-137: Have tidal current measurements from the Arc5km2018 model been verified in this region?

The Arc5km2018 has not been verified in this region. However, as far as we know, AOTIM5 (5km horizontal resolution Arctic Ocean Tidal Inverse Model) and its recent version developed in 2018 (Arc5km2018) are the best available estimates of the tidal forcing in the Arctic Ocean. Arc5km2018 has been improved compared to AOTIM5 as:
(1) it uses an improved prior model with ocean open boundary forcing from an updated TOPEX/Poseidon global barotropic global tide solution (TPXO9.1)
(2) it adds four tidal constituents, 2N2 and the three non-linear constituents
(3) it assimilates much longer time series of altimetry, notably from the ESA satellites that sample to 81.5 degrees north. (from https://arcticdata.io/catalog/view/doi:10.18739/A21R6N14K)

- L143-146: These lines about the number of profiles could be moved into the methods section (2.1).

Agreed, we moved these lines at the end of section 2.1.

- L156-160: These lines seem out of place here.

We agree that these lines are out of place here. We added these sentences rather to the introduction

- L178-180: Equation 5 doesn't represent the surface layer depth from Randelhoff et al. (2017). It represents the scaled vertical coordinate those authors use, and the surface layer depth corresponds to a specific value of r. This isn't clear in your text.

Yes indeed you are right, r is not the surface layer depth but rather a scaled depth coordinate, but as suggested in the following comment, we deleted these details.

- L178-183: There is a lot of detail here for a surface layer definition that you ultimately don't use. This could be simplified by trimming out a number of intervening sentences and leaving only the beginning and end: "We also estimate a surface layer depth following Randelhoff et al. (2017); however, the mixed layer depth and the surface layer depth are very similar (not shown), so in the rest of the study. . .".

Agreed. We deleted the details about the surface layer definition.

- L186-187: This warm water is difficult to identify in the sections (especially panels a and c).

We agree that it is a bit hard to identify the warm Atlantic Water in the panels. We now also refer to figure 4a (blue line) that show better the warm Atlantic Water. We also added a thicker 2 degree temperature contour in Figure 3 to emphasize the Atlantic Water layer.

- L191-193: Are these averages of profiles from both July and September cruises? If not, which set are these? Please clarify in your text. Also, if surface stratification and buoyancy flux are significantly different in July and September (e.g., section 4.1), then I would expect the shallow parts of those profiles to be fairly distinct between seasons and not appropriate to average. Ensure that you comment on that in the text.

The average is calculated using profiles from both July and September cruise. Surface stratification and buoyancy flux are indeed different in July and September, but these profiles are mainly used to discuss the deeper water column and not the upper 50 m. We now clarify this in the text.

'We calculated average profiles of temperature, salinity, dissipation rate and diffusivity using data combined from both July and September cruises. The averaging is made in isopycnal coordinates to account for the possible vertical displacement of isopycnals and water masses from the slope to the deep basin. Once averaged, the profiles are mapped onto vertical coordinate using the corresponding average depth of an isopycnal (Figure 4). While this averaging is representative of the vertical structure below the mixed layer, it is probably not appropriate for the surface layer where surface stratification and buoyancy flux are significantly different in July and September (see following section for more details).'

- Figure 3: The red line showing mixed-layer depth is very difficult to see. In the left panels, it blends into the temperature field and in the right panels it is obscured by other details. This is also partly due to how close to the surface the mixed layer is relative to the scale of the plot. In the left panels, the scale in the upper 100m differs from the rest of the plot to better show upper ocean details, but they are still hard to see and the scale change could be further exaggerated. I did not immediately realize that the vertical scale change was not included in the right panels. I would also appreciate if the Atlantic water was somehow better identified or more visible in this figure – I don't clearly see it in all sections.

Yes, indeed this figure contains a lot of information and some details cannot be identified easily. We made an attempt to improve the presentation. We changed the color of the mixed layer depth to dark green. To better indicate the location of the Atlantic Water, we added a thicker white contour for the 2°C isoline. We also changed the vertical scale of the figure and now zoom in the upper 600 m. The vertical scale is now similar between both right and left panels.

- Figure 4: Some of the subfigure tick-labels are overlapping and hard to read. The legend is small and difficult to read. Also, it may be helpful to replace legend labels with “inshore, shelf break, offshore” as are used in the text. It’s difficult to see the details in the upper water column (below ∼100m); you may consider using a different vertical scale (as in figure 3), or providing insets that zoom in on the surface of each panel.

Thanks for all these comments to improve the figure. We now make sure that subfigure tick-labels do not overlap. We changed the legend labels too. These panels are presented to give an overview of the average profiles at depth, and do not aim at focusing in the upper ocean. We therefore do not present split panels with a zoom in on the surface.

- L206-208: Here you say that the core of the Atlantic water current is between 400 m and 600 m, but in L186-187 you associate the Atlantic water with 500 m to 1100 m depths. Throughout the text you use the 800 m isobath as a reference for Altantic water, which is consistent with L186-187 but not with L206-208. Please clarify this and ensure consistency throughout.’

The core of the Atlantic Water current is indeed between 400 and 600 m depth in the water column. L186-187 we stated that the Atlantic Water core is between the 500 and 1100 m depth isobaths (spatial/horizontal location, not vertical location).

- L208: The only mention of current measurements throughout the rest of the paper are the modeled tidal currents, but this sentence is about water column currents. Are these measured with a shipboard ADCP during the cruise? Or is this sentence a reference to known characteristics of the Atlantic water layer from other studies (e.g., the submitted work by Kolås et al., that you reference in L196)?

Yes indeed this sentence is a reference to known characteristics of the Atlantic water layer from other studies. We added the reference to Kolås et al. (2020).

- L250-256: The non-linear dependence of mixed-layer dissipation on wind energy input is a really interesting result, but it would be valuable to explore this concept in more detail and relate it to prior studies (either here, or in some part of the discussion). In particular, there has been some theory that looks at this relation in the wave-boundary layer and may or may not support a linear relationship (see Craig & Banner, 1994, doi: 10.1175/15200485(1994)024<2546:MWETIT>2.0.CO;2 and Thomson, 2016, doi: 10.1175/JPO-D-15-0130.1). It’s also been considered in a bulk sense in the mixed layer (i.e., as an efficiency; see Sutherland et al., 2013 doi:10.5194/os-9-597-2013 and references therein; though this is still in the wave-breaking framework). I think there might be some richness in the fact that this analysis suggests a non-linear relationship and worth speculating about why or what that might mean (perhaps stratification or mixed-layer depth play in in some way). Additionally, it may be worth mentioning the wave conditions during the sampling in section 3.1, even if only qualitatively.

Wave measurements were performed during the cruise in September and are shown in Løken, Trygve K., et al. "Wave measurements from ship mounted sensors in the Arctic marginal ice zone."

arXiv preprint arXiv:1911.07612 (2019). On average the waves were about 1 m (significant wave height) during the September cruise. Unfortunately, we are missing microstructure data in the upper layer where surface wave effects are important. The VMP needs several meters to adjust to free-fall, and the measurements are performed next to the ship, the wake of which contaminates the dissipation measurements. We do not aim to resolve the surface-wave induced processes with our dataset and cannot quantify the role of the wave-boundary layer dynamics on the observed non-linear dependence of mixed-layer dissipation on wind energy input. We added in the manuscript:

In the section 'environmental conditions':
'During the cruise in September, surface gravity waves were estimated using single point ocean surface elevation data obtained from the bow of the ship using a system that combines an altimeter and inertial motion unit (Løken et al., 2019). The significant wave height varied between 0.5 and 1.5 m with mean wave periods between 2 and 6 s."

In the section 'wind forcing':
"During the cruise in September, the surface waves were characterized by 0.5-1.5 m significant wave height (Sect. 3.1, Løken et al., 2019). Because the dissipation measurements are contaminated by the ship's wake in the upper 10 m, we cannot resolve the role of wave-boundary layer dynamics on the vertical structure of dissipation. Since the wave forcing in September was weak, we do not expect a substantial contribution to the observed non-linear dependence of mixed-layer dissipation on wind energy input. However the relatively large values of Dml in July when E10 was large (circles in Figure 6) might be associated with surface waves.'

- Section 4.2: In this section you take all of the data together, but in section 4.1 you contrast some of the details of the mixed-layer between the July and September cruises. Am I correct in interpreting from figure 6 and L252-253 that there's not enough data in September to be able to make meaningful comparisons of Dml between seasons? If it's possible to contrast the effects of wind forcing between the two seasons at all, it would be very interesting.

Indeed, there are so few data points in September in the mixed layer that we are not able to make a meaningful comparison of Dml between seasons.

- Figure 6: Are there any noticeable relationships if you colour the points by mixed-layer depth?

Below is the figure 6 with the points colored by the mixed layer depth. There is no obvious relation that warrants further investigation.

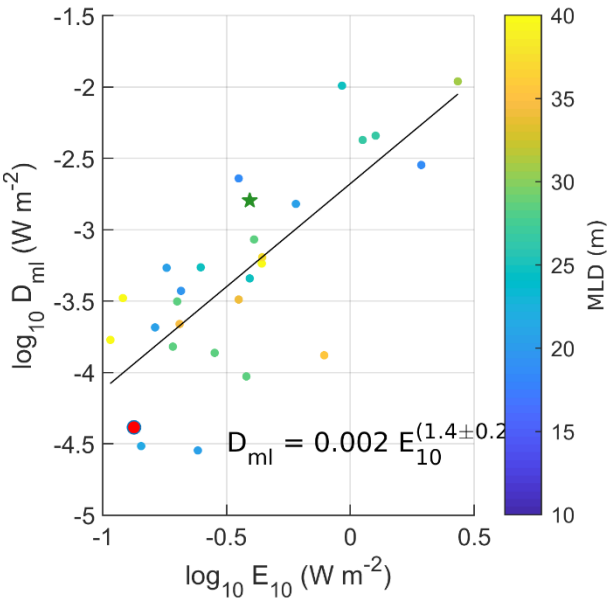

Figure 1. As in Figure 6 but color-coded for the mixed layer depth.

- L316: What are the confidence intervals on the decay scales? Are 18 m and 22 m statistically different from each other?

Both decay scales are statistically different from each other. The 95% confident level is about 2m. We added the confidence interval in the text.

- L320: “We investigate the role of two distinct contributions from tidal currents”. Contributions to what? This sentence isn’t clear.

We clarify this sentence: ‘We investigate the role of two distinct contributions from tidal currents to the turbulent mixing’.

- L326: Why the choice of 250 m for integrating the dissipation? Is this choice informed in any way by the estimated decay scales from earlier? Are results sensitive to other choices?

We chose 250 m as this is the depth where dissipation rate decrease in Figure 8. We tested the sensitivity to different choices (e.g., integrating up to 3 or 5 decay length scales). Although the regression coefficients vary, same trends are observed.

- L330-331: Why exclude wave (tidal) frequency?

We agree that we should have taken into account the tidal wave frequency. We recalculated using the 4 main tidal components (M2, S2, O1, K1), including their corresponding frequencies in the analysis. The contribution from each constituent (using the cross-isobath component of predicted tidal current at the time and location of each station) is summed up to obtain the new data points. The result is shown in Figure 2a. Because we removed these calculations from the paper, we do not describe in detail here. Overall, the new calculations using the frequency dependence are very similar to the original calculations. However, as suggested in the next comment, we decided to remove this panel as the tidal work does not correlate well with D250.

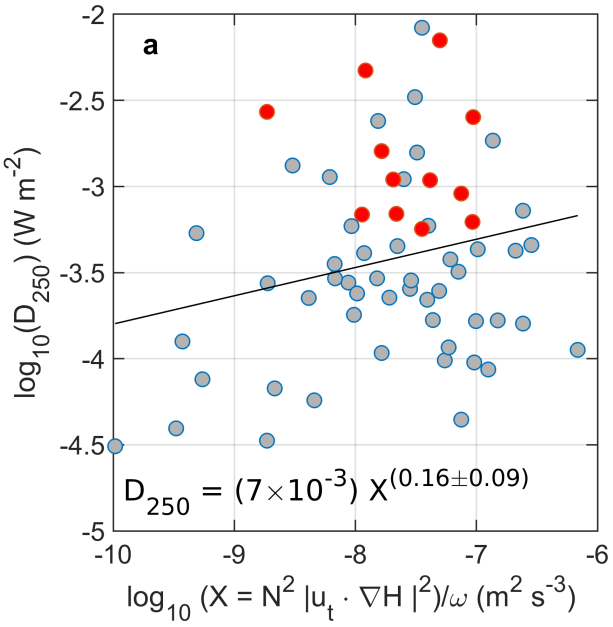

Figure 2: Depth-integrated dissipation rate in the bottom 250 m regressed against the instantaneous (using u_t) values of a tidal-work related parameter, summed over 4 main tidal components (M2, S2, O1, K1). Linear fits on logarithmic parameter space (i.e., power-law fits) are the black lines and the corresponding equations are indicated with the 95% confidence levels. Red dots are the data points from the RS2 station. Process stations are batch-averaged (in sets of 4-5 consecutive profiles) in panel a.

- L327-347: Since the tidal-work parameter in equation 7 doesn't provide a useful correlation, you could choose to simplify the text and figure 9 by removing some of the text in the section, and simply stating that you also tried comparing D250 with the rate of work given by Nash et al., (2006) but found no significant correlation. Then you could remove equation 7 and some of the text surrounding it and remove panels a and b from figure 9. This is a personal choice, but it would better highlight your positive results.

We agree that the tidal-work parameter does not provide a useful correlation. As suggested, we simplified the text and figure 9 and simply stated that D250 and the tidal work do not correlate well.

- L335: It's worth highlighting somewhere that equation 8 is analogous to the equation for E10 (in section 4.2), and so the nonlinear relationship between D250 and Wbotdrag is something that can be related to the nonlinear relationship between Dml and E10.

Yes indeed it is valuable to highlight that equation 8 is analogous to the equation for E10.
Below Eq (6), we inserted:
"Note that this equation is analogous to the drag relation for the wind energy flux E10 (in section 4.2)."

In line 314 we added:
'This nonlinear relationship between D_250 (dissipation in the bottom 250 m) and W_botdrag shows parallels with the nonlinear relationship between D_ml (dissipation in the surface mixed layer) and E_10'

- L350: Does it make sense to compare the bottom drag coefficient to one from the Bering Strait? I wouldn't assume that the bottom morphologies of the two areas would be similar. Can you instead refer to a range of "typical" bottom drag values?

We cite the bottom drag coefficient estimated in the Bering Strait because it is a relevant estimate that was done in the Arctic Ocean from in situ turbulent observations. We now also refer to the typical bottom drag values:

"This value is comparable to but smaller than the typical range of bottom drag values of (1-3) x 10^{-3} and the bottom drag deduced from in situ observations in Bering Strait… …."

- Figure 9: I don't quite understand why there is only one red dot in panels b and d but many in panels a and c? Is this due to how you perform the u_rms calculation?

The u_rms calculation is performed at a given location, hence the RS2 data points are only one dot in the computation of the u_rms.

- L367-368: If you are showing only a line along the Eurasian Basin, then "Pan-Arctic" in the section title is not appropriate. (Note, the authors have already expressed plans to rename this section).

Yes we agree and we changed the title to 'Estimates of tidally-driven dissipation rate in the Eurasian Basin'.

- L399-400: Maybe highlight to what extent the dissipation in panel b of Figure 10 will account for the nonlinear waves (e.g., if it did account for it, I'd expect to see peaks in D250 in panel b that correspond to the peaks of inverse Fr in panel c). Make it explicit that these are areas that warrant specific further study.

Thanks for this suggestion. We inserted:
'In the region north of Svalbard and in the eastern part of the Laptev Sea, the large depth-integrated dissipation rate observed in Figure 10b can be driven by nonlinear waves implied by the peaks of inverse Fr (Figure 10c). These two areas warrant further studies. In the eastern part of the Kara Sea, however, the depth-integrated dissipation rates are relatively low despite the large inverse Fr values that suggest nonlinear processes could develop there.'

- L387-405: While the discussion of these potential non-linear wave "hotspots" is very interesting, it feels somewhat disconnected from the rest of the study. Most of the times non-linear waves present in the results before this point are references to the high dissipation event at RS2 that was already documented by Fer et al. (2020b). This section would connect more if you make more explicit comparisons between the general results and the non-linear wave results (e.g., you have RS2 points in red in figure 9, which show the associated increase in D250, but those points are presented as more of a sidenote in the text L351-353 when there's potential to make more direct comparisons).

We connected the two sections better by adding a cross-reference to Fig 8 and also given the value for the inverse Fr at RS2. We inserted:
'The increase in dissipation rate driven by these nonlinear waves is also noticeable in Figure 8a and c (the red dots). At this location, the inverse Froude number for the diurnal frequency exceeds 3,

supporting the interpretation that such conditions can favor the development of nonlinear processes.'

- Section 7.1: Overall, this is a nice extension of the ideas in section 6.

Thanks

- Section 7.2: As written, there is no clear link between the ideas in the section and the results you've presented. Do your results agree with or refute any of the studies you cite? Can they be compared at all? This section provides interesting background and motivation, but without linking it explicitly to your results it is not really a discussion section. (Note, the authors have already expressed plans to remove this section).

Indeed, we agree that there is no clear link between the ideas in the section and the results we have presented. For this reason, we decided to remove this section.

- Section 7.3: Similar to section 7.2, this provides good background but isn't otherwise well linked to the rest of the study.

We agree that this section was not well linked to the rest of the study. We reformulated and connected this section better with our results. We revised the last 3 paragraphs:

'Ivanov and Timokhov (2019) estimated that from the Yermak Plateau to the Lomonosov Ridge, 41% of the Atlantic Water heat is lost to atmosphere, 31% to deep ocean and 20% is lost laterally. Heat loss resulting from vertical heat fluxes contributes to the heat loss to atmosphere and to deep ocean, but not to the lateral heat loss. Several processes can lead to lateral heat loss North of Svalbard, including eddy spreading from the slope into the basin (Crews et al., 2018; Våge et al., 2016). Using eddy-resolving regional model results, Crews et al. (2018) found that eddies export 1.0 TW out of the boundary current, delivering heat into the interior Arctic Ocean at an average rate of $\sim$15W m^{-2}. West of Svalbard, Kolås and Fer (2018) found that the measured turbulent heat flux in the WSC was too small to account for the cooling rate of the Atlantic Water layer, but reported substantial contribution from energetic convective mixing of an unstable bottom boundary layer on the slope. Convection was driven by Ekman advection of buoyant water across the slope, and complements the turbulent mixing in the cooling process. The estimated lateral buoyancy flux was about 10^{-8} W kg^{-1} (Kolås and Fer, 2018), sufficient to maintain a large fraction of the observed dissipation rates, and corresponds to a heat flux of approximately 40 W m^{-2}. We can expect similar processes to extract heat and salt from the Atlantic Water core north of Svalbard. Such processes can explain why turbulent heat fluxes are only responsible for 10% of the Atlantic heat loss north of Svalbard. Furthermore, large heat loss during extreme events should not be ignored. For example, Meyer et al. (2017) found that the average heat flux of about 7 W m^{-2} across the 0°C isotherm increased during storms, exceeding 30 W m^{-2}. During our survey without extreme wind events, the turbulent heat fluxes represent only a small portion of the heat loss of the Atlantic Water.'

- L459-460: The different values of kappa_bot may be a stronger result to highlight in the summary than the different decay scales (or maybe include both?)

We added the values of kappa_bot in the summary: 'The vertical decay scale of the diffusivity is 22 m for those strong tidal currents, compared to 18 m for weaker tidal currents; the bottom diffusivity is larger with strong tidal currents than for weaker ones (1×10^{-3} m^2s^{-1} and 7×10^{-4} m^2s^{-1} respectively)'

Technical corrections
- L25-26: Awkward grammar/sentence structure in the sentence starting with “The heat reservoir. . .”.

We changed the sentence: ‘The heat contained in the Atlantic and Pacific origin waters has the potential to melt the entire sea ice if reaching the surface’

- L41-42: Do you have the correct reference for the sentence “Wind-driven momentum input. . .”? Is this meant to reference Rainville and Woodgate (2009) instead of Rainville and Windsor (2008)?

Yes, indeed there was a mistake in the reference. We corrected it.

- L154: “encounter” should be “encountered”

Thanks, corrected

- L317: In the sentence “We use kappa_bot. . .”, should that instead be kappa_bg?

Yes indeed it should be kappa_bg, we corrected it.

- L414: Awkward grammar/sentence structure in the sentence starting with “They found. . .”.

This section is now deleted.

Response to referee #1
This manuscript presents a particularly interesting set of turbulence observations from north of Svalbard in the Arctic that cover the 2018 summer and autumn period. The authors investigate the vertical structure of mixing, heat fluxes and seasonal changes, and identify the processes driving the variability in the turbulence field. Both the wind and tidal supplies of energy are estimated with parameterizations derived and discussed. An attempt to extrapolate to the whole Eurasian Basin is made and interesting areas are identified that could be investigated in further work. The current lack of turbulence measurements in the Arctic is highlighted as the main limitation to pan-Arctic parameterization as well as the difficulty in accounting for lateral processes and fluxes, and for extreme events such as storms. The quality of the English in the text is excellent. The Abstract and Introduction are good, the Data & Methods and Observations sections are excellent. The Upper layer Dynamics section is fine. The section on Mixing in the AW layer is very interesting. The Tidal Mixing section presents a very nice analysis and tools. The Discussion is hard to link to this particular study’s findings. The Summary section is excellent. The figures are excellent and have great detail. It was a pleasure to read through this work.

Thanks for these comments

Major comments:
-Introduction: Sort out the introduction part on the various sources and intensity of turbulence in the Arctic (see individual comments further down).

Agreed. We rearranged the introduction as suggested below

-Discussion: Currently the discussion section reads in parts (see individual comments) more like a literature review than a discussion around how your findings fit in current research and their wider impact and implications. You have excellent results and just need to rewrite this section a little. In its current form, the manuscript is already very good and presents a trove of findings for this region on the topic of turbulence. However, the manuscript would benefit from some sorting in parts, better highlight of key findings throughout (done well in the Summary), and better framing of this study's results in the discussion. I recommend that the manuscript is accepted subject to minor revision and look forward to seeing a revised version.

We have rearranged the discussion as suggested below

Individual comments
Abstract:
- Well written overall. The first sentence could do with rewriting to better reflect the beginning of your introduction. Right now you fit too much in that sentence and loose some of the meaning.

We changed the first sentence of the introduction: 'The Arctic Ocean has major implications on global scale as the Arctic Ocean is a main sink for heat and salt. Ocean mixing contribute to this sink by mixing the Atlantic and Pacific-origin waters with surrounding waters.'

1.Introduction:
- L23: You state 'In the near future we may enter a new regime, in which the interior Arctic Ocean is entirely ice free in summer and sea ice is thinner and more mobile in winter'. I would argue that 'may' here is inappropriate and 'will' is more suitable. 'May'creates doubts around the likelihood of this happening. Please rephrase to better reflect current research findings such as the latest estimate from Guarino et al. (Guarino,M., Sime, L.C., Schröeder, D. et al. Sea-ice-free Arctic during the Last Interglacialsupports fast future loss. Nat. Clim. Chang. (2020). https://doi.org/10.1038/s41558-020-0865-2) of 2035 for first ice free summer, or average from CMIP6 models of 2046 with a range of roughly 2030-2065.

We changed 'may' to 'will' and we added the reference Guarino et al., 2020

- L31-37 and L38-46: In both these paragraphs, you describe the various sources and intensity of mixing in the Arctic. These two sections could do with merging and a better ordering of the different sources and intensity discussed.

We merged the two paragraphs and we ordered better the sources and intensities. We also removed part of the description of the sources and intensities as we found that it did not serve the rest of the manuscript.

- L65: Consider adding the following reference somewhere here: 'The lack of sea ice is mainly due to heat from the Atlantic layer reaching the surface'. Duarte, P., Sundfjord A., Meyer, A., Hudson, S. R., Spreen, G., & Smedsrud, L. H. (2020). Warm Atlantic water explains observed sea ice melt rates north of Svalbard. Journal of Geophysical Research: Oceans, 125, e2019JC015662. https://doi.org/10.1029/2019JC0156622.

We added the reference

2.Data and Methods:

- L105: Unclear what ‘In total, we collected 31 profiles.’ Do you mean ship CTD profiles? Or VMP profiles or ? This doesn’t match other number of VMP profiles stated earlier in the manuscript.

Thanks for spotting this mistake. We deleted this sentence

- L126: Pls define ‘g’ in equation (4) if not previously defined.

We added the definition of g: ‘where alpha and beta are respectively the thermal expansion and salinity contraction coefficients, and g is the gravitional constant.’

L129-130: You state here that ‘We used the profiles collected from the ship’s CTD system (Sea-Bird Scientific,SBE 911plus on both cruises) to check and correct the temperature and salinity from the VMP’. But earlier on L107 you state ‘A good agreement was observed and no correction was made.’. Please rewrite to make both statement consistent.

Thanks for pointing it out. We deleted ‘correct’ in the first sentence.

3.Overview of observations:
- L172-173: Unsure you need this statement here considering you have explained it clearly it in the figure caption.

Agreed. We deleted this sentence

- Figure 3: Add what the red line is MLD in the caption.

We added in the caption that the (now) green line is the mixed layer depth.

4. Upper layer dynamics:
- L252: Add the definition of Dml in the text. Currently it only appears in Fig.6 caption. Can you make it clearer in the text how you obtained your estimate of the relationship between Dml and E10: it’s a linear fit of Dml from the VMP data and E10 from the shipwind speed measurements.

We added the definition of Dml and clarify that we apply a linear fit

5. Mixing in the Atlantic Water layer:
- L264: Should ‘in present conditions of a warming Arctic’ not be ‘in the new conditions of a warming Arctic’?

Changed as suggested.

- Fig.7 is great

Thanks!

- L274-275: This statement is confusing ‘vertical turbulent heat fluxes are negative(less than 5Wm-2)’ You might want to rephrase to ‘vertical turbulent heat fluxes are negative (0 to -5Wm-2)’

Changed as suggested.

- L282: Which section are you speaking about when you say '...the heat loss due to vertical turbulent heat fluxes is about... across the section'?

We are talking about the cross-isobath section. We agree that 'across the section' is more confusing than helpful and we deleted it.

- L282-285: Why is your estimate of heat loss due to vertical turbulent heat fluxes(1.2x10ˆ5 W/m) so much lower than Kolas estimates from the same cruise (9.1x10ˆ7W/m and 9.6x10ˆ6 W/m)?

Here we estimate the heat loss only due to vertical turbulent heat fluxes. Kolås et al. (2020) estimate the along-path change of heat content, that takes into account not only the vertical turbulent heat fluxes but also the other fluxes that can impact the heat content.

6. Tidal mixing:
- Fig. 8 caption: 'Average profiles of a) dissipation rate, b) turbulent heat flux and c) diapycnal diffusivity k for small' Also add Espi and F_H after the variable's names.

Done

- L326-366: Nice analysis of the vertically integrated dissipation rate in bottom 250m.

Thanks

7. Discussion:
- Fig.10 caption: I suggest removing the first word 'Typical'. Also, what is the back-ground shading on the small map, topography? This map is useful and should be listed in the caption.

'Typical' reinforce the idea that we use u_rms. The background shading on the small map is topography, we added this information in the caption.

- L358: Subsection title 'Pan-Arctic estimates of tidally-driven dissipation rates' is not representative of results presented which are 'instead of presenting Arctic-wide maps we concentrate on the Eurasian Basin from north of Svalbard into the East Siberian Sea'. Please change section title to represent better the content. Also edit L355 in the previous section announcing the 'pan-Arctic estimate'.

We changed the title of the subsection to 'Estimates of tidally-driven dissipation rate in the Eurasian Basin' and we edited l.355: 'An Eurasian-basin coarse estimate will be given ...'.

- L398-405: Great findings.

Thanks

- L410: Rephrase sentence 'In the future, sea ice meltwater is expected to increase and turbulent mixing near the surface to decrease' to better justify/explain the expected decrease in mixing (due to increase stratification).
- L 423: 'and an earlier onset of stratification which might be indirectly linked to bloom development'...due to.... Please add details.

- Section 7.2: I m unsure about the contribution your results make in this theme of ‘impact of meltwater on the near surface mixing’. Consider better linking to your observations or moving this section as context in your introduction in a condensed form.

We agree that this discussion is not really relevant to our analysis. We deleted section 7.2.

- L433: I m unsure about how this statement ‘Vertical turbulent heat fluxes are not the main source of cooling of the Atlantic Water layer in the Arctic. Ivanov and Timokhov (2019) reviewed that from the Yermak Plateau to the Lomonosov ridge, 41% of the Atlantic Water heat is lost to the atmosphere, 31% to the deep ocean and 20% is lost laterally.’ fits with the previous ‘heat loss due to turbulent vertical mixing represents less than 10% of the total heat loss of the Atlantic Water’ . Would the 10% not be part of the 31% deep ocean and 20% laterally? You seem to imply they are different when you state ‘Vertical turbulent heat fluxes are not the main source of cooling of the Atlantic Water layer in the Arctic’. Please tidy up these two paragraphs so the reader can follow your thoughts. Again, further down you discuss eddies and their roles. But is the heat export from eddies not included in the 20% lost laterally from Ivanov and Timokhov (2019)?

Yes, you are right. We are mixing different informations. We found that turbulent vertical mixing represents less than 10% of the total heat loss of the Atlantic Water layer, but indeed we do not specify where the heat is lost, so these 10% are not to be compared with the percentages from Ivanov and Timokhov (2019). We changed the sentence: ‘
Ivanov and Timokhov (2019) estimated that from the Yermak Plateau to the Lomonosov Ridge, 41% of the Atlantic Water heat is lost to atmosphere, 31% to deep ocean and 20% is lost laterally. Heat loss resulting from vertical heat fluxes contributes to the heat loss to atmosphere and to deep ocean, but not to the lateral heat loss. ’

- L444 and 445: The numbers you quote there (10ˆ-8 and 40W/mˆ2), are they from Kolas and Fer or from this study? Again, how does this section of the discussion(7.3 AW heat loss) exactly links with your findings. Currently this reads a lot like an (excellent) literature review, rather than you putting your new findings in context...

These numbers were from Kolås and Fer. We agree that this section looks more like a literature review, and we tried to better put our new findings in context. We mainly changed the last 2 paragraphs:

‘West of Svalbard, Kolås and Fer (2018) found that the measured turbulent heat flux in the WSC was too small to account for the cooling rate of the Atlantic Water layer, but reported substantial contribution from energetic convective mixing of an unstable bottom boundary layer on the slope. Convection was driven by Ekman advection of buoyant water across the slope, and complements the turbulent mixing in the cooling process. The estimated lateral buoyancy flux was about 10^{-8} W kg^{-1} (Kolås and Fer, 2018), sufficient to maintain a large fraction of the observed dissipation rates, and corresponds to a heat flux of approximately 40 W m^{-2}. We can expect similar processes to extract heat and salt from the Atlantic Water core north of Svalbard. Such processes can explain why turbulent heat fluxes are only responsible for 10% of the Atlantic heat loss north of Svalbard. Furthermore, large heat loss during extreme events should not be ignored. For example, Meyer et al. (2017) found that the average heat flux of about 7 W m^{-2} across the 0°C isotherm increased during storms, exceeding 30 W m^{-2}. During our survey without extreme wind events, the turbulent heat fluxes represent only a small portion of the heat loss of the Atlantic Water.’

8. Summary:

- L459-460: Consider adding ‘The vertical decay scale of the diffusivity is 22m *for those strong tidal currents*, compared to 18m for weaker tidal currents.’

Thanks, done

- L470: Consider adding details ‘More in situ observations from different sites *in the Eurasian Basin and elsewhere in the Arctic* are needed to confirm our results.’

Thanks, done

- L475: Can you add ‘of the *expected/estimated* total heat loss of the Atlantic Water layer’.

We added ‘estimated’

- L475-476: Can you explain better the relation between the first part of the sentence and the later part? I understand you mean to say that increased vertical mixing during storms might partially close the budget but don’t make up the whole ‘missing’ heat loss which might be mostly lateral fluxes. So that both lateral fluxes and extreme conditions such as storms, frontal systems etc should be investigated. But this will not super clear in the current form of the sentence.

We reformulate the last sentence: ‘Increased vertical mixing during storms would add to this figure. However, integrated studies addressing lateral mixing processes, frontal systems as well as extreme conditions such as storms are needed to close the heat budget in this region.’

Structure and drivers of ocean mixing north of Svalbard in summer and fall 2018

Zoe Koenig[1,2], Eivind H. Kolås[1], and Ilker Fer[1]

[1]Geophysical Institute, University of Bergen and Bjerknes Center for Climate Research, Bergen, Norway
[2]Norwegian Polar Institute, Tromsø, Norway

Correspondence: Zoe Koenig (zoe.koenig@uib.no)

Abstract. ~~Ocean mixing in the Arctic Ocean cools and freshens~~ The Arctic Ocean is a main sink for heat and salt for the global ocean. Ocean mixing contributes to this sink by mixing the Atlantic and Pacific-origin waters ~~by mixing them~~ with surrounding waters~~, which has major implications on global scale as the Arctic Ocean is a main sink for heat and salt~~. We investigate the drivers of ocean mixing north of Svalbard, in the Atlantic sector of the Arctic, based on observations collected during two research cruises in summer and fall 2018. Estimates of vertical turbulent heat flux from the Atlantic Water layer up to the mixed layer reach 30 W m^{-2} in the core of the boundary current, and average to 8 W m^{-2}, accounting for $\sim 1\%$ of the total heat loss of the Atlantic layer in the region. In the mixed layer, there is a nonlinear relation between the layer-integrated dissipation and wind energy input; convection was active at a few stations and was responsible for enhanced turbulence ~~compare~~ compared to what was expected from the wind ~~work~~ stress alone. Summer melting of sea ice reduces the temperature, salinity and depth of the mixed layer, and increases salt and buoyancy fluxes at the base of the mixed layer. Deeper in the water column and near the seabed, tidal ~~work~~ forcing is a main source of turbulence: diapycnal diffusivity in the bottom 250 m of the water column is enhanced during strong tidal currents, reaching on average 10^{-3} m^2 s^{-1}. The average profile of diffusivity decays with distance from seabed with an e-folding scale of 22 m compared to 18 m in conditions with weaker tidal currents. A nonlinear relation is inferred between the depth-integrated dissipation in the bottom 250 m of the water column and the tidally-driven bottom drag, and is used to estimate the bottom dissipation along the continental slope of the Eurasian Basin. Computation of ~~the~~ an inverse Froude number suggests that nonlinear internal waves forced by the diurnal tidal ~~activity~~ currents (K_1 constituent) can develop north of Svalbard and in the Laptev and Kara Seas, with the potential to mix the entire water column vertically. ~~Estimates of vertical turbulent heat flux from the Atlantic Water layer up to the mixed layer reaches 30 W m^{-2} in the core of the boundary current, and is on average 8 W m^{-2}, accounting for $\sim 1\%$ of the total heat loss of the Atlantic layer in the region.~~

1 Introduction

The Arctic Ocean is a sink for salt and heat. Relatively warm and salty Atlantic waters enter the Arctic Ocean via Fram Strait and the Barents Sea through-flow, and colder and fresher Arctic waters exit flowing east of Greenland through the East Greenland Current. Annual average water mass transformation in the Arctic is about -0.62 ± 0.23 in salinity and -3.74 ± 0.76°C in temperature (Tsubouchi et al., 2018). With the rapid and large sea ice decline, the Arctic Ocean is particularly vulnerable to climate change. In the near future we ~~may~~ will enter a new regime, in which the interior Arctic Ocean is entirely ice free in summer and sea ice is thinner and more mobile in winter (Guarino et al., 2020), which will have vast implications for the Arctic ocean circulation, the marine ecosystems it supports, and the larger-scale climate (Timmermans and Marshall, 2020). The heat ~~reservoir that contains~~ contained in the Atlantic and Pacific origin waters has the potential to melt the entire sea ice if reaching the surface (Maykut and Untersteiner, 1971). The estimated mean Arctic Ocean surface heat flux necessary to keep the sea ice thickness at equilibrium is 2 W m^{-2} (Maykut and McPhee, 1995), yet observations indicate mean surface heat fluxes of 3.5 W m^{-2} (Krishfield and Perovich, 2005). To assess the evolution of the sea ice, the oceanic heat in the Arctic must be monitored and understood.

Atlantic Water is a main component of the Arctic Ocean heat budget, with particular influence in the Atlantic sector. An important player in the transformation of the Atlantic Water is vertical mixing. ~~In the Arctic Ocean, vertical mixing is dominated by turbulence generated by processes over topography and along margins (Padman and Dillon, 1991; Lenn et al., 2011; Rippeth et al., 2015 while the~~ The central Arctic is relatively quiescent (Fer, 2009; Lincoln et al., 2016). Microstructure measurements indicate turbulent kinetic energy dissipation in the halocline of the deep basins to be around 10^{-10} to 10^{-9} W kg^{-1} (Fer, 2009; Lincoln et al., 2016; Rippeth et al., 2015). The dissipation rates are estimated to be ~~2~~ several orders of magnitude larger on the ocean margins than over the abyssal plain ~~, for example about $3 - 20 \times 10^{-8}$ W kg^{-1} in the region just north of Svalbard (Rippeth et al., 2015)~~(Padman and Dillon, 1991; Lenn et al., 2011; Rippeth et al., 2015; Fer et al., 2014).

~~Vertical mixing in the Arctic Ocean is driven by various energy sources, such as winds, tides and mesoscale activity. Zhao et al. (2014) described a prevalent Arctic eddy field, typically generated by instability of surface fronts (in the eastern Canada basin) or instability of boundary currents (in the southwestern Canada Basin or in the vicinity of ridge features and in shelf regions in the Eurasian Basin). Topographic waves generated over bathymetric slopes and rough topography, forced by the tides, are the main source of energy for increased tidal dissipation rates observed over topography (Padman et al., 1992; Rippeth et al., 2017 Wind-driven momentum input to the Arctic ocean is largely dampened by sea ice cover (Rainville and Winsor, 2008). In winter months with complete ice cover, inertial wave energy and shear are generally weaker than in summer when we observe an increased atmosphere to ocean momentum transfer in open water regions (Dosser and Rainville, 2016).~~

North of Svalbard is a location with enhanced mixing~~in the Arctic~~. It is also a key region for the Arctic Ocean heat and salt budget, as it is the gateway for the Fram Strait inflow of Atlantic Water. The circulation of Atlantic Water here is complex, with several recirculations in Fram Strait and three main inflow branches including the Yermak Branch (YB, Cokelet et al. (2008)), the Yermak Pass Branch (YPB, Koenig et al. (2017); Crews et al. (2019); Menze et al. (2019)) and the Svalbard Branch (SB,

Cokelet et al. (2008)), all originating from the West Spitsbergen Current (WSC) (Figure 1a). As the Atlantic Water flows eastward, it deepens, gets colder and fresher due to mixing with the surrounding waters.

Cooling and freshening of the Atlantic Water north of Svalbard result from different processes. Along the slope north of Svalbard, eddies are shed from the Atlantic Water Boundary Current (Våge et al., 2016; Crews et al., 2018), transporting 0.16 Sv (1 Sv = 10^6 m^3 s^{-1}) of Atlantic Water and 1.0 TW (1 TW = 10^{12} W) away from the boundary current. ~~At depth, the ocean is affected by the tidal work:~~ Large vertical turbulent fluxes can occur in localized regions. Strong tidal currents over bathymetric slopes and rough topography generate internal waves which are a main source of energy for increased turbulence dissipation rates (Padman et al., 1992; Rippeth et al., 2017; Fer et al., 2020b). Rippeth et al. (2015) showed that the Yermak Plateau is a hot spot for tidal mixing~~and~~ . Fer et al. (2014) suggested that in ~~the region~~this region, almost the entire volume-integrated dissipation can be attributed to the ~~dissipation~~ loss of baroclinic tidal energy converted locally from the surface tides. In the Nansen Basin north of Svalbard, turbulence in the upper layer influences the sea ice cover. Peterson et al. (2017) found an average winter ocean-to-ice heat flux of around 1.4 W m^{-2} , with episodic local upwelling events and proximity to Atlantic Water pathways increasing the heat fluxes by one order of magnitude. Meyer et al. (2017) presented 6 months of turbulence data collected from January to June 2015 during the N-ICE2015 campaign. The combination of storms and shallow Atlantic Water leads to the highest heat flux rates observed: ice-ocean interface heat fluxes averaged 100 W m^{-2} during peak events.

In the last decade~~in the Barents Sea first and then in the Eurasian Arctic Ocean~~, ice-free regions have been observed along the path of the Atlantic Water, ~~and~~ in the Barents Sea first and then in the Eurasian Arctic Ocean, with warm and saline water ~~has been~~ extending up to the surface (Årthun et al., 2012; Ivanov et al., 2016). The lack of sea ice is mainly due to heat from the Atlantic layer reaching the surface (Duarte et al., 2020), and is associated with the Atlantification of the Eurasian Basin and of the Barents Sea (Polyakov et al., 2017; Årthun et al., 2012). In the Eurasian Basin, the upward oceanic heat flux towards the mixed layer has increased from $3-4$ W m^{-2} in 2007 - 2008 to more than 10 W m^{-2} in 2016 - 2018 (Polyakov et al., 2020). This process is called the ice-ocean heat feedback as the increased ocean heat flux to the sea surface reduces ice thickness and increases its mobility, increasing atmospheric momentum flux into the ocean and reducing the damping of surface-intensified baroclinic tides (Polyakov et al., 2020). Mixing north of Svalbard is of particular interest to understand the Atlantification as it contributes to the cooling and freshening of the Atlantic Water entering the Arctic Ocean. The reduced ice cover over the continental slope north of Svalbard can be seen as a precursor of the entire Eurasian Basin and the processes therein. Indeed, Polyakov et al. (2020) documented an eastward lateral propagation of the so-called Atlantification, with a lag of about 2 years between the Barents Sea and the eastern Eurasian Basin. Therefore, detailed observations of the ocean dynamics north of Svalbard are needed to evaluate the active processes modifying the Atlantic Water layer in a changing Arctic, and their potential influence on the sea ice.

In this study we present observations of ocean turbulence north of Svalbard collected in summer and fall 2018, and focus on mechanisms which lead to turbulence in the different layers of the water column. Two main sources of ocean mixing are investigated: the wind and the tidal forcing. Turbulence production by background shear will not be addressed in this study as the vertical resolution (8 m) of the current data collected during the cruises is not sufficient to resolve shear instabilities.

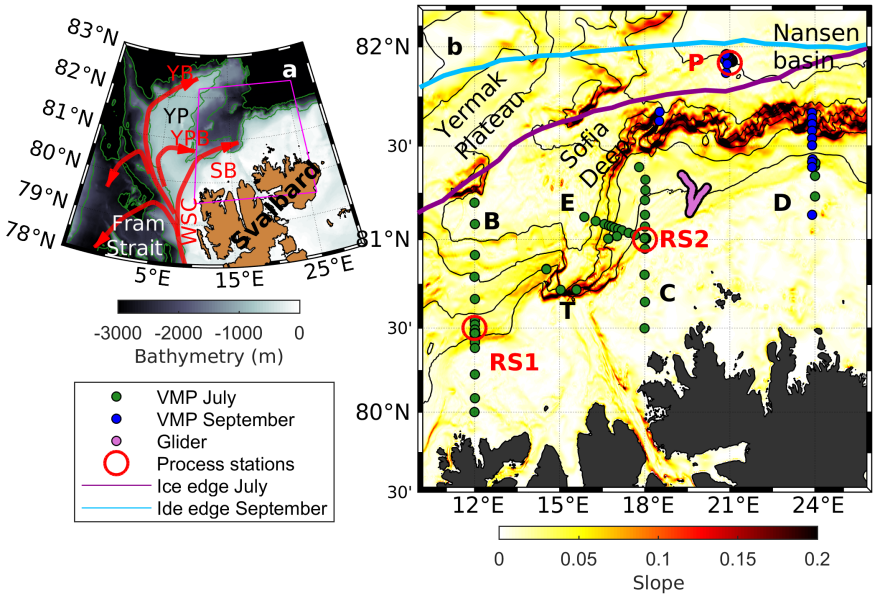

Figure 1. a) Circulation pattern of Atlantic Water around Svalbard, with the West Spitsbergen Current (WSC), the Svalbard Branch (SB), the Yermak Branch (YB) and the Yermak Pass Branch (YPB). Bathymetry is from the International Bathymetric Chart of the Arctic Ocean, IBCAO-v3 (Jakobsson et al., 2012). b) Close-up on the magenta box in panel a. Station locations (~~June~~July, green dots; September, blue dots), sections (B, C, D and E), and process stations (red circles marked RS1, RS2 and P) are shown. The slope steepness calculated from IBCAO-v3 is color-coded at the background. Isobaths are drawn every 1000 m in (a) and 500 m in (b). Purple/light blue lines are the averaged sea ice edge defined as the 15% ice concentration over the summer ~~/~~and fall cruise, respectively.

2 Data and methods

Data were collected in 2018, during two cruises that took place north of Svalbard as a part of the Nansen Legacy Project. The summer cruise was on *R/V Kristine Bonnevie* from 27 June to 10 July 2018 (Fer et al., 2019), while the fall cruise was on the ice-class *R/V Kronprins Haakon* from 12 to 24 September 2018 (Fer et al., 2020a). During the cruises, several sections were repeated north of Svalbard across the continental slope, and 3 stations (two in July and one in September) were occupied for about 24 h to study mixing processes (Figure 1b). Turbulence profiles were collected during both cruises (185 profiles in 9 days in July and 43 in 5 days in September) using a Vertical Microstructure Profiler (VMP). We ~~use the International Thermodynamic Equations of Seawater (TEOS-10) (McDougall and Barker, 2011) with~~ calculated the Conservative Temperature (Θ) and Absolute Salinity (S_A) using the International Thermodynamic Equations of Seawater (TEOS-10) (McDougall and Barker, 2011).

Table 1. Overview of ocean microstructure measurements. The number of profiles used in analyses is n, after batch-averaging repeat profiles in the process stations.

Start	End	Instrument	Number of profiles	n
30 Jun 2018 17:30 UTC	08 Jul 2018 20:00 UTC	VMP 2000	185	76
16 Sep 2018 21:30 UTC	20 Sep 2018 04:40 UTC	VMP 2000	43	14

2.1 Vertical Microstructure Profiler (VMP)

We used a 2000 m-rated VMP manufactured by Rockland Scientific, Canada (RSI). The VMP is a loosely tethered profiler with a nominal fall speed of $0.6\ \mathrm{m\,s^{-1}}$. The profiler was equipped with pumped Sea-Bird Scientific (SBE) conductivity and temperature sensors, a pressure sensor, airfoil velocity shear probes, one high-resolution temperature sensor, one high-resolution micro-conductivity sensor and three orthogonal accelerometers. The microstructure data were processed using the routines provided by RSI (ODAS v4.01). Assuming isotropic turbulence, the dissipation rate of turbulent kinetic energy per unit mass, ϵ, can be expressed as

$$\epsilon = 7.5\nu\overline{\left(\frac{\partial u}{\partial z}\right)^2} \tag{1}$$

where ν is the kinematic viscosity equal to about $1.6\times10^{-6}\ \mathrm{m^2\ s^{-1}}$ in these temperatures, overbar denotes averaging in time and $\partial u/\partial z$ is the small-scale shear of one horizontal velocity component u. Dissipation rates were calculated from the shear variance obtained by integrating the shear vertical wavenumber spectra in a wavenumber range that is relatively unaffected by noise, and corrected for the variance in the unresolved portions of the spectrum using an empirical model (Nasmyth, 1970). The shear spectra were computed using 1 s Fourier transform length and half-overlapping 4 s segments. We quality screened the resulting values by inspecting the instrument accelerometer records, individual spectra and individual dissipation rate profiles from the two shear probes. We averaged estimates from both probes, except when their ratio exceeded 10, for example as a result of plankton hitting a sensor, the lowest estimate was chosen. Noise level of the dissipation rate measured by the VMP is about $(2-3)\times10^{-10}\ \mathrm{W\,kg^{-1}}$. The temperature and salinity data from the VMP were compared against the ship's SBE CTD profiles. A good agreement was observed and no correction was made. ~~In total, we collected 31 profiles.~~ Dissipation measurements from the upper 15 m were excluded because of the disturbance from the ship's keel ~~,~~and the profiler's adjustment to free fall. The vertically integrated dissipation rate over a layer h (surface mixed layer or near-bottom layer in the following sections) is defined as $D_h = \rho_0\int_h \epsilon(z)dz$ (in $\mathrm{W\ m^{-2}}$) where $\rho_0 = 1027\ \mathrm{kg\,m^{-3}}$ is the seawater reference density.

We estimated the turbulent heat flux F_H from

$$F_H = -\rho_0 C_p \kappa \frac{\partial \Theta}{\partial z}, \tag{2}$$

where $C_p = 3991.9\ \mathrm{J\,kg^{-1}\,K^{-1}}$ is the specific heat of seawater, Θ is the background temperature and κ is the diapycnal eddy diffusivity. We thus assume that turbulence diffuses the finescale temperature gradient at the same rate as the density gradient. The sign convention is that positive heat fluxes are directed upward in the water column.

We expressed the diapycnal diffusivity κ ~~as a function of turbulent activity index,~~ following Bouffard and Boegman (2013), where three states (energetic, transitional and buoyancy-controlled) are defined depending on the ~~Reynolds number~~ buoyancy Reynolds number, $Re_b = \frac{\epsilon}{\nu N^2}$. In the transitional range ($8.5 < Re_b < 400$), calculation of κ is identical to Osborn (1980), using the canonical mixing coefficient of 0.2 (Gregg et al., 2018); however in the energetic regime the latter is an overestimate. In our dataset, 80% of the estimates are in the transitional regime. To compute κ, the buoyancy frequency or Brunt Väisälä frequency, N, was calculated using $N^2 = -\frac{g}{\rho_0}\frac{\partial \sigma_0}{\partial z}$, where g is the gravitational acceleration and σ_0 is the potential density anomaly referenced to surface pressure. Background vertical gradients (for temperature, salinity and density) were taken over a 10-m length scale. ~~As~~ To prevent spuriously large values of κ as N approaches neutral stratification, ~~κ attains very large values. The estimates of κ in~~ segments with buoyancy frequency below a noise level of $N^2 = 10^{-7}\ \mathrm{s^{-2}}$ were excluded.

We also computed the ~~salinity~~ salt flux F_S and the buoyancy flux F_B~~, with the same sign convention as the turbulent heat flux~~:

$$F_S = -\rho_0 \kappa \frac{\partial S_A}{\partial z}, \tag{3}$$

$$F_B = -g(\beta F_S - \alpha F_H), \tag{4}$$

where α and β are respectively the thermal expansion and salinity contraction coefficients, g is the gravitational constant, and the positive fluxes are directed upward.

In the rest of the study, sets of 3-4 consecutive repeat profiles at the process stations are averaged to avoid any bias toward these stations. Table 1 lists two numbers of 'profiles': the total number of casts performed (number of profiles) and the number of profiles used in analyses (n) after batch-averaging of consecutive repeat profiles. In the rest of the study, we always refer to the number of profiles after batch-averaging (in figures 4 and 7).

2.2 Other datasets

We used the profiles collected from the ship's CTD system (Sea-Bird Scientific, SBE 911plus on both cruises) to check ~~and correct~~ the temperature and salinity from the VMP. CTD data were processed using the standard SBE post-processing software, and salinity values were corrected against water sample analyses. Pressure, temperature and practical salinity data are accurate to ± 0.5 dbar, $\pm 2 \times 10^{-3}$ °C, and $\pm 3 \times 10^{-3}$, respectively.

The wind speed, direction and surface air temperature (Figure 2) were recorded every minute during the cruises from the ship's weather station. The wind energy flux from the atmosphere into the ocean is estimated from the wind speed at 10 m height (U_{10}) as: $E_{10} = \tau U_{10} = \rho_{air} C_d U_{10}^3$ (Oakey and Elliott, 1982), where ρ_{air} is the density of air and τ is the wind stress, parameterized using a quadratic drag with a drag coefficient C_d. We use the neutral drag coefficient at 10 m computed following

Large and Pond (1981), adjusting the wind speed measured at 15 m height in July and 22 m height in September from the ship's mast to 10 m.

We used Arc5km2018 (Erofeeva and Egbert, 2020), a barotropic inverse tidal model on a 5-km grid, to estimate the tidal currents using the 8 main constituents (M_2, S_2, N_2, K_2, K_1, O_1, P_1, Q_1) and 4 nonlinear components (M_4, MS_4, MN_2, and $2N_2$).

Bathymetric contours shown in maps are from the International Bathymetric Chart of the Arctic Ocean (IBCAO-v3) (Jakobsson et al., 2012). Station depths are from the ship's echosounder.

To discuss our findings in a broader scope, we used the global monthly isopycnal mixed-layer ocean climatology (MIMOC) at $0.5°$ resolution, which is objectively mapped with emphasis on data from the last decade (Schmidtko et al., 2013).

3 Overview of observations

~~In the rest of the study, sets of 4-5 consecutive repeat profiles at the process stations are averaged to avoid any bias toward these stations. Table 1 lists two numbers of 'profiles': the total number of casts performed (number of profiles) and the number of profiles used in analyses (n) after batch-averaging of consecutive repeat profiles. In the rest of the study, we always refer to the number of profiles after batch-averaging (in figures 4 and 7).~~

3.1 Environmental context

The cruises cover the summer and fall conditions, typically in open waters. Four main sections were occupied north of Svalbard: Section B, C and E in July, and section D in September, capturing the core of the inflowing Atlantic Water. Selected stations were occupied for 24 hours to investigate mixing processes in detail at a specific location: T, RS1, RS2 and P (Figure 1b). In September, turbulence profiling terminated after the winch broke, resulting in fewer profiles (section D, process study P and the outer deep stations at section C).

In July, the Yermak Plateau was covered by sea ice and the ice edge was close to the continental slope north of Svalbard (Figure 1), limiting the station coverage (e.g., section D could not be completed). We note that the sea ice ~~encounter~~ encountered in July was closer to the continental slope at 24°E than what is suggested by the sea ice edge from satellite, defined here as 15% sea ice concentration. In September, the sea ice edge was $\sim$ 30 to 50 km further north, and the continental slope was entirely free of ice ~~. Open water conditions on shelves were previously observed to~~ which can facilitate enhanced wind energy input to the oceanic near-inertial currents (Rainville and Woodgate, 2009). ~~The momentum transfer from the wind is also affected by ice conditions in deep basins. The drifting Ice-Tethered Profiler dataset in the Canada Basin from 2005 to 2014 shows that the near-inertial internal wave field is the most energetic in summer when sea ice is at a minimum (Dosser and Rainville, 2016).~~

Air temperature differs between the two cruises: while it was mainly positive in July, the temperature dropped to -10°C in September (Figure 2a and d) near the sea ice edge. Over the two cruises, wind was moderate, peaking only for half a day to 15 m s^{-1} on 7 July (Figure 2b). In September, the average wind speed was 8 m s^{-1} with no specific events. During the cruise in September, surface gravity waves were estimated using single point ocean surface elevation data obtained from the bow of the

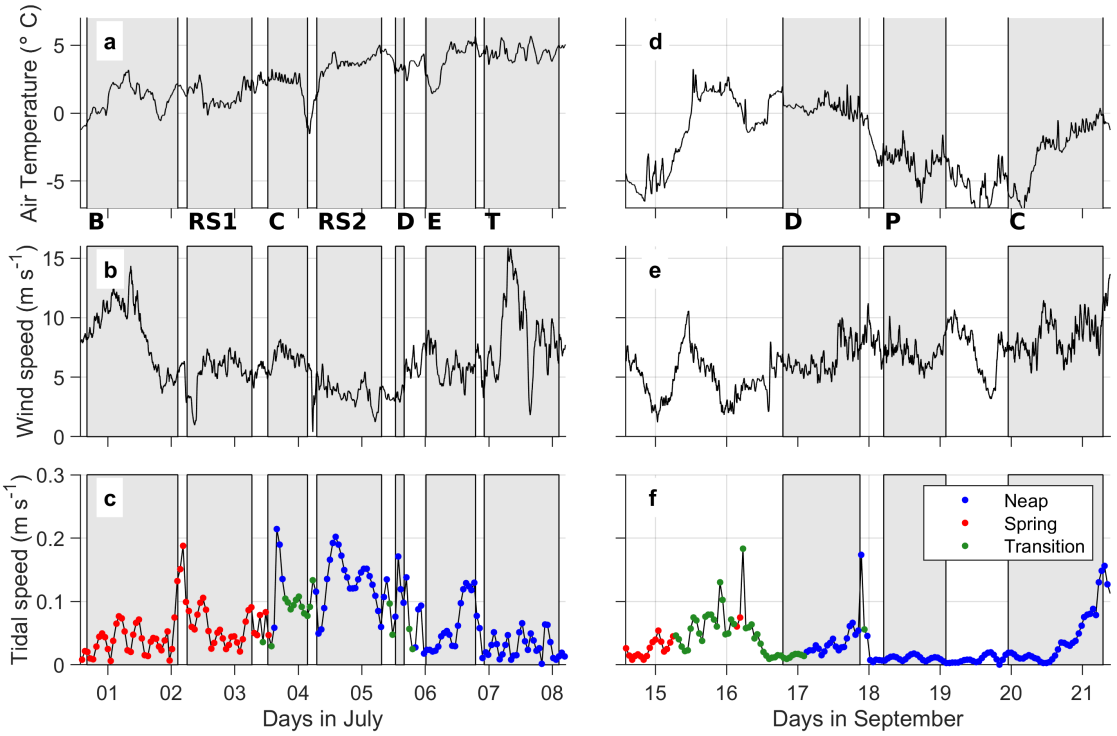

Figure 2. Air temperature (a and d), wind speed (b and e) from the ship's weather station and tidal current speed (c and f) from the Arc5km2018 model. Left panels are during the July (Summer) cruise. Right panels are during the September (fall) cruise. Grey shadings correspond to the periods of turbulence measurements (sections or process stations). In panel c and f, the tidal conditions during time of sampling are indicated as neap, spring tide and the transition between the neap and spring tide with blue/red/green dots respectively.

ship using a system that combines an altimeter and inertial motion unit (Løken et al., 2019). The significant wave height varied between 0.5 and 1.5 m with mean wave periods between 2 and 6 s.

Tidal currents varied significantly during the cruise depending on the location, with a maximum amplitude about 20 cm s^{-1} during RS2 from 4 to 6 July. The tidal currents were stronger on the slope than in the deep basin (such as during P in the Nansen Basin). In July, sections were occupied during spring tides for the first 3 days and during neap tides for the rest of the cruise. In September, the tidal currents at the stations were weaker and mainly during neap tides, except for a short period of spring tides in the beginning of the cruise (around 15 September 2018).

3.2 Hydrography

Figure 3 shows the distribution of temperature and dissipation rate collected in sections and the process stations performed during the two cruises. Temperature sections were obtained by gridding the data in 1 km horizontal and 2 m vertical grid size

~~. Note that in Figure 3, the horizontal axis in the left panels (sections) is distance to the 800 m isobath (negative onshore and positive offshore), and time in the right panels (process stations)~~using linear interpolation.

We estimate the mixed layer depth (~~red~~ dark green line in Figure 3), as the depth at which the density exceeds the shallowest measurement by 0.01 kg m^{-3} in July, and by 0.03 kg m^{-3} in September, because of the presence of melt water at the surface in September. The vertical gradients are large, and the mixed layer depth is not very sensitive to the exact ~~criteria. We also estimate~~ criterion. An estimate of a surface layer depth ~~following Randelhoff et al. (2017):~~

$$r(z) = \frac{\sigma_0(z) - \sigma_{0s}}{\Delta\sigma_0}$$

~~where $\Delta\sigma_0 = \sigma_{0d} - \sigma_{0s}$ is the surface density deviation, σ_{0d} is the density averaged between 55 and 65 m and σ_{0s} is the density averaged between 5 and 8 m. The surface layer depth is useful when there is no well-defined mixed layer but a seasonal pycnocline. In our dataset, $\Delta\sigma_0$ is typically larger than 0.02 kg m^{-3}, hence the surface layer is discernibly affected by meltwater (Randelhoff et al., 2017); however the surface density deviation is larger in September: the meltwater layer is deeper and fresher in fall than in summer. Here, the mixed layer depth and the surface layer depth are very similar~~ (not shown) ~~. In the rest of the study, we use the mixed layer depth using the density difference criterion (red line in Figure 3)~~following Randelhoff et al. (2017) was very similar.

The slope north of Svalbard is characterized by Atlantic Water flowing along the 800 m isobath. The Atlantic Water is defined as water masses with $\Theta > 2$°C and $27.7 < \sigma_0 < 27.97$ kg m^{-3} following Rudels et al. (2000). The warm waters observed roughly between 500 and 1100 m isobaths are associated with the Atlantic Water core (section panels in figure 3 and blue line in figure 4a). Colder and fresher waters found offshore are Atlantic Water from Fram Strait, which has been modified by mixing with the surrounding waters. A thorough description of the hydrography and circulation during the two cruises can be found in Kolås et al. (2020).

We calculated average profiles of temperature, salinity, dissipation rate and diffusivity using data combined from both July and September cruises. The averaging is made in isopycnal coordinates ~~,~~ to account for the possible vertical displacement of ~~the isopycnals and of the~~ isopycnals and water masses from the slope to the deep basin. Once averaged, the profiles are mapped ~~into~~ onto vertical coordinate using the corresponding average depth of an isopycnal (Figure 4). While this averaging is representative of the vertical structure below the mixed layer, it is probably not appropriate for the surface layer where surface stratification and buoyancy flux are significantly different in July and September (see following section for more details). The average profiles are obtained in subsets, depending on their distance from the 800 m isobath, which is representative of the mean location of the core of the inflowing Atlantic Water (Kolås et al., 2020). The core of the Atlantic Water current typically extends about 20 km onshore and offshore of the 800 m isobath (Kolås et al., 2020). However, in order to characterize the different regions of the slope with comparable number of profiles in each region, we present averages inshore of -10 km, within $\pm$10 km of the 800 m isobath and offshore of 10 km (Figure 4).

Averaged temperature and salinity profiles are very similar at depth (below 600 m, around 0° C and 35.1 g kg^{-1}, Figure 4e), and the main differences are observed in the upper 200 m. The 'inshore' average profile is the warmest with a temperature

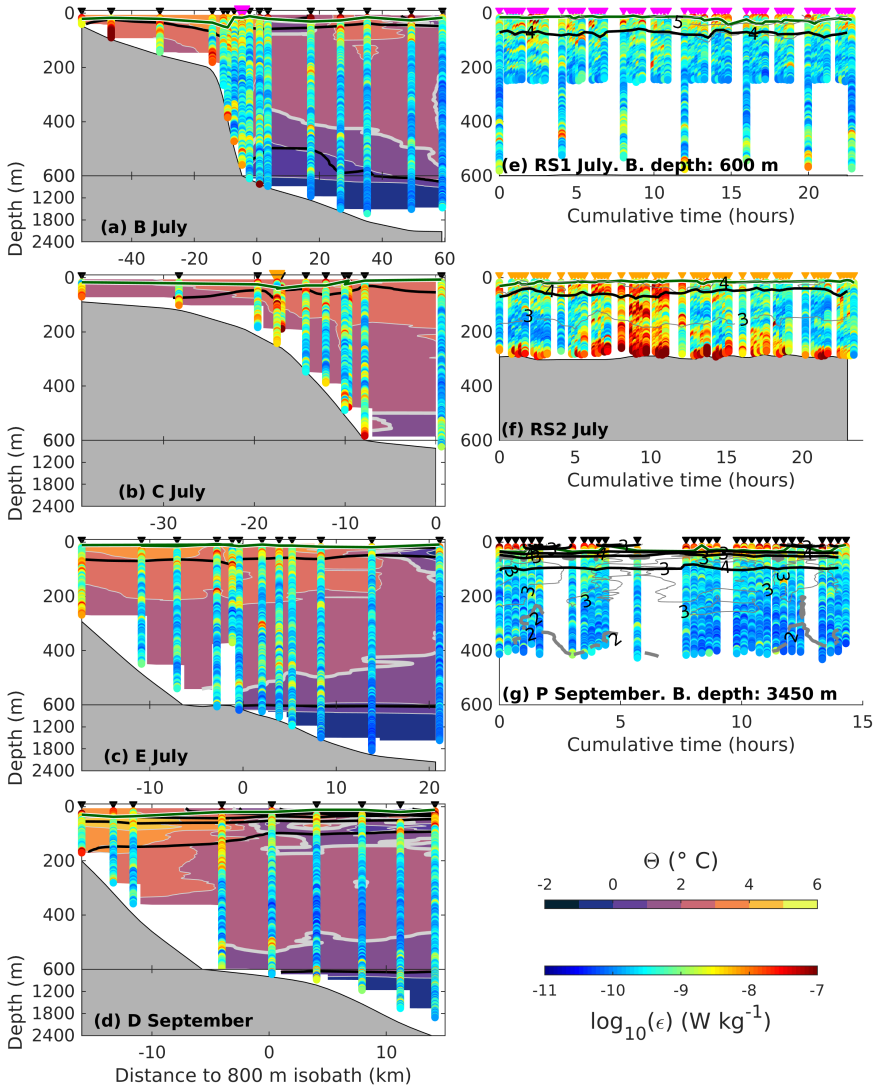

Figure 3. Overview of the main sections (left panels) and ~~of~~ the process ~~studies~~ study stations (right panels) during the July and September cruises. In the left panels, background is ~~Conservative Temperature~~Θ, superimposed are the dissipation rate profiles (ϵ). Note the change of vertical scale at ~~100~~ 600 m depth. In the right panels, temperature contours as shown as thin grey lines. In all panels, bold black lines are the isopycnals and the thicker grey line is the 2°C isotherm. Bathymetry is from the bottom depth measured at each station. Triangle markers are the time/location of the stations. In panels a and b, the pink and orange station markers indicate the location of the RS1 and RS2 process station, respectively, shown in panels e and f. At station P (g), one early VMP cast performed about 6 h before the start of the first shown profile is excluded. The horizontal axis is the distance to the 800 m isobath in the left panels and cumulative time from the first profile in the right panels. The dark green line is the mixed layer depth.

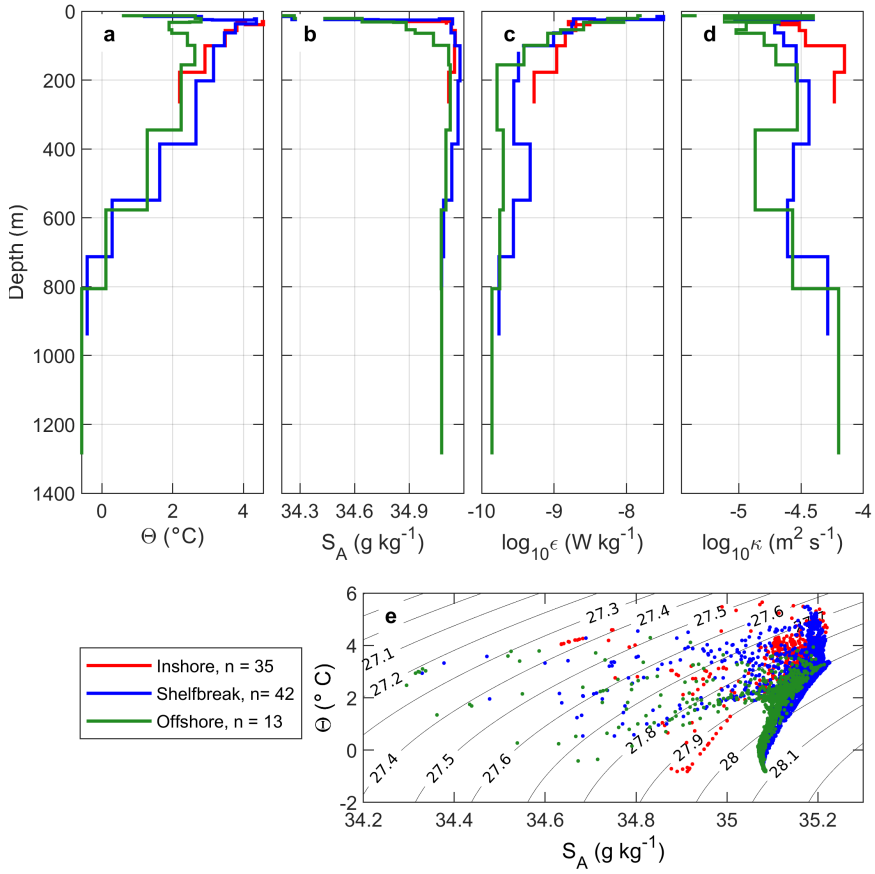

Figure 4. Isopycnally-averaged profiles of a) Θ, b) S_A, c) dissipation rate, ϵ and d) diapycnal diffusivity, κ. The profiles are shown using the average depth of the isopycnals. e) Temperature-Salinity diagram. Profiles are selected relative to distance from the 800-m isobath: inshore of -10 km (red), at the shelf break in the Atlantic Water core (blue), and offshore of 10 km (green). In the legend, n indicates the number of batch-averaged profiles used in each average.

maximum of ~ 5.5°C at around 75 m depth. The 'offshore' average profile has the coldest mixed layer (around 0°C) and the coldest core of Atlantic Water (around 2°C), a characteristic of the hydrography in the Nansen Basin (Kolås et al., 2020).

3.3 Turbulence

230 On average, dissipation rates are the largest in the upper ocean, reaching 10^{-7} W kg^{-1} near the surface and decreasing rapidly with depth (Figure 4c). In deeper layers, the dissipation rates are larger inshore than offshore, decreasing from 5×10^{-10} W kg^{-1} on the shallows (red profiles) to 10^{-10} W kg^{-1} on the deep offshore profiles (green profiles). Between 400 and 600 m depth, a local maximum in dissipation rate is observed in the core of the inflowing Atlantic Water current (blue profiles), where

the strongest currents are observed (Kolås et al., 2020). Diffusivity is large in both the mixed layer and at depth close to the bottom (Figure 4d), exceeding 6×10^{-5} m^2 s^{-1}.

Of the microstructure measurements collected during the cruises, the process stations RS2 and P were analyzed and reported in detail in Fer et al. (2020b) and Koenig et al. (2020), respectively. The largest dissipation rates were measured at RS2, with high dissipation rates observed in the whole water column during a 6-h turbulent event (Figure 3f), caused by an intense dissipation of lee waves driven by cross-slope tidal currents (Fer et al., 2020b). Process station P in the Nansen Basin far from the continental slope (Figure 1) is a 24 h process study at a surface thermohaline front (Figure 3g). At this specific station, turbulence structure in the mixed layer was generally consistent with turbulence production through convection by heat loss to atmosphere and mechanical forcing by moderate wind (Koenig et al., 2020).

In the following sections, we will first examine the mixed layer evolution from summer to fall and the role of wind forcing. Then we will investigate the ~~sources of turbulence at depth within and below~~ turbulence structure in the deeper layers, forced by tidal currents. Using the measurements in the Atlantic Water layer we quantify the vertical heat loss from the Atlantic Water layer. Basic statistics (arithmetic and geometric mean and standard deviations) of mixing parameters for July and September are summarized in Table 2. We used both arithmetic and geometric mean to describe the dissipation rates, diffusivity and turbulent fluxes. For variables with lognormal distribution (such as ϵ and κ), the geometric mean (GM) characterizes the distribution's central tendency while the arithmetic mean (AM) tends to be disproportionately skewed by a small number of large values (Scheifele et al., 2020). AM characterizes the integrated effect of the distribution and is representative of the cumulative effect of mixing and average buoyancy transformations produced by mixing (Scheifele et al., 2020).

4 Upper layer dynamics

4.1 Seasonal evolution

Solar heating melts the sea ice, which has consequences for the upper ocean dynamics. Throughout the summer, the mixed layer becomes fresher and lighter (34.9 g kg^{-1} and 27.7 kg m^{-3} in July, and 34 g kg^{-1} and 26.95 kg m^{-3} in September, figure 5), and also deepens (18 m in July and 23 m in September). This evolution in summer towards a lighter mixed layer is mainly due to the meltwater during the summer. In both summer and fall, dissipation rates, buoyancy fluxes and turbulent heat fluxes increased at the base and just below the mixed layer compared to the rest of the water column (figure 5 and table 2).

The depth-integrated dissipation rate at the base of the mixed layer D_{ml} is on average about $(1-2) \times 10^{-4}$ W m^{-2} ~~in both cruises~~during both cruises, with a geometric mean of about 3×10^{-5} W m^{-2} (table 2). ~~In both July and September downward turbulent buoyancy fluxes and upward turbulent salinity fluxes are observed~~ Turbulent buoyancy fluxes in the mixed layer ~~.~~ ~~Salinity~~ are directed downward, and turbulent salt fluxes upward, in both July and September. Salt and buoyancy fluxes are larger in September than in July at the base of the mixed layer: ~~salinity~~ salt flux is 4.2×10^{-4} ~~W kg~~kg s^{-1}m^{-2} in July and 1.1×10^{-3} ~~W kg~~kg s^{-1}m^{-2} in September and buoyancy flux is -2.4×10^{-9} W kg^{-1} in July and -5.3×10^{-9} W kg^{-1} in September, as the meltwater content in the upper layer is larger in September than in July.

Table 2. Statistics of the turbulence variables measured in July and September. AM: arithmetic mean, GM: geometric mean, σ: standard deviation, D_ϵ: vertically integrated dissipation rate, ϵ: dissipation rate, κ: diffusivity, F_H: vertical turbulent heat flux (positive upward). Four layers are defined. MLD: ± 10 m around the base of the mixed layer, AW_{core} - MLD: from the Atlantic Water core to the mixed layer depth, AW layer: in the Atlantic Water layer, and AW_{core} - bottom: from the Atlantic Water core to the seafloor. The geometric mean is ill-defined for negative values hence not provided for the turbulent heat fluxes.

		July			Sept		
		AM	GM	σ	AM	GM	σ
$D_\epsilon \times 10^{-4}$ (W m^{-2})	MLD	1.3	0.3	2.5	1.8	0.3	4.6
	AW_{core} - MLD	3.1	0.6	7.2	3.8	0.7	8.3
	AW layer	8.9	5.0	12.8	8.7	4.8	12.8
	AW_{core} - bottom	9.3	6.2	12	9.6	6.4	12.0
$\epsilon \times 10^{-9}$ (W kg^{-1})	MLD	23.7	5.3	56.5	28.4	5.5	67.6
	AW_{core} - MLD	18.8	4.4	50.1	22.6	4.8	55.5
	AW layer	4.1	1.7	10.3	4	1.7	10.3
	AW_{core} - bottom	3.9	1.5	10.3	3.9	1.6	10.3
$\kappa \times 10^{-5}$ (m^2 s^{-1})	MLD	6.9	3.9	6.9	38	4	221
	AW_{core} - MLD	5.4	2.6	7.7	16.6	3.0	64.8
	AW layer	10.9	7.6	13.3	9.8	6.5	13.2
	AW_{core} - bottom	11.1	7.9	13.3	10.5	7.4	13.1
F_H (W m^{-2})	MLD	2.5	~~X~~ n/a	18.4	3.6	~~X~~ n/a	17.6
	AW_{core} - MLD	4.4	~~X~~ n/a	11.4	3.0	~~X~~ n/a	8.9
	AW layer	-1.4	~~X~~ n/a	1.6	-1.4	~~X~~ n/a	1.7
	AW_{core} - bottom	-1.5	~~X~~ n/a	1.6	-1.4	~~X~~ n/a	1.6

Turbulent heat fluxes across the base of the mixed layer are positive (upward) in both July and September, but larger in September than in July (3.6 W m^{-2} and 2.5 W m^{-2} respectively). The turbulent heat fluxes measured during both cruises are comparable to what is observed under the sea ice ~~without any specific forcing~~ in the absence of forcing events during the N-ICE2015 experiment (Meyer et al., 2017; Peterson et al., 2017) (about 2 W m^{-2}), but about 1/40 to 1/30 times the heat fluxes (up to 100 W m^{-2}) observed during storm events above the continental slope. Variations in the density field ~~in the Arctic~~ are dominated by the variations in salinity, thus buoyancy and ~~salinity~~ salt fluxes vary concomitantly.

4.2 Wind forcing

Wind stress at the ocean surface is one of the main drivers for the upper layer turbulence and can increase the ocean-to-ice heat fluxes (Meyer et al., 2017; Dosser and Rainville, 2016). ~~The~~ A fraction of the wind energy flux from the atmosphere ~~into the ocean can be estimated from the wind speed at 10 m height (U_{10}) as: $E_{10} = \tau U_{10} = \rho_{air} C_d U_{10}^3$ (Oakey and Elliott, 1982), where ρ_{air} is the density of air and τ is the wind stress, parameterized using a quadratic drag with a drag coefficient C_d. We~~

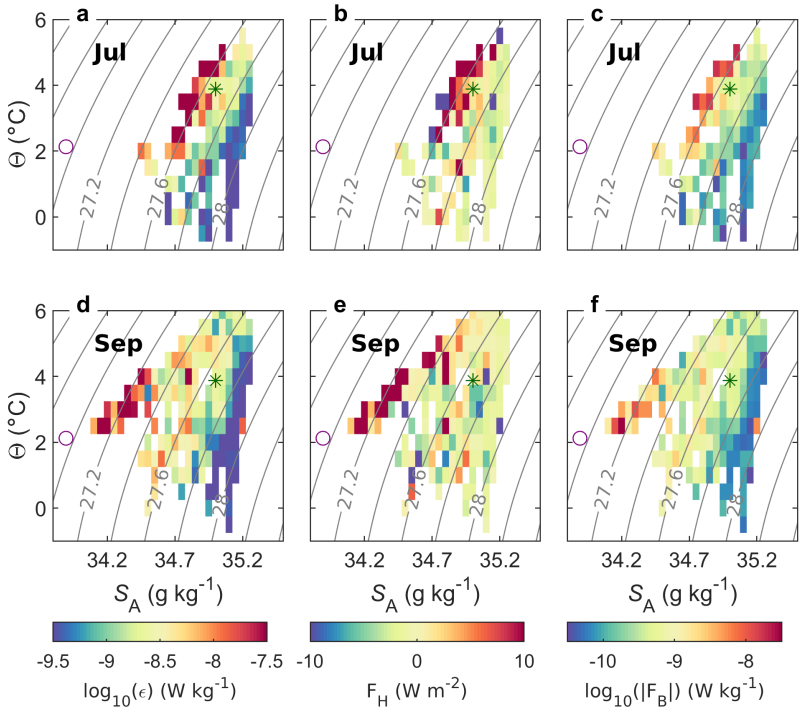

Figure 5. Temperature-Salinity diagrams where the color-coded bins are dissipation rate (a and d), turbulent heat flux (b and e) and magnitude of buoyancy flux (c and f, the buoyancy fluxes are all oriented downward). Contours are σ_0, referenced to surface pressure. Panels a, b and c are for summer (July cruise) and panels d, e and f for fall (September cruise). The green star is the mean temperature and salinity property of the mixed layer in July and the purple circle is the corresponding value in September.

~~use the neutral drag coefficient at 10 m computed following Large and Pond (1981), adjusting the wind speed measured at 15 m height in July and 22 m height in September from the ship's mast to 10 m. A fraction of this energy flux~~ to the ocean then fuels turbulence in the upper ocean and is dissipated in the mixed layer. Using the observed dissipation in the mixed layer and the wind energy input ~~north of Svalbard~~ (Figure 6), we obtain a linear fit: $D_{ml} = 0.002 E_{10}^{(1.4\pm0.2)}$, where D_{ml} is the depth-integrated dissipation rate in the mixed layer. Observations in September are limited as only a few stations were performed with the VMP.

For relatively low values of E_{10} (less than 6.3×10^{-1} W m^{-2}), the relation is almost linear, suggesting that about 1 per mille of wind energy input is dissipated in the mixed layer. For larger E_{10}, additional processes such as breaking gravity waves can contribute. During the cruise in September, the surface waves were characterized by 0.5-1.5 m significant wave height (Sect. 3.1, Løken et al. (2019)). Because the dissipation measurements are contaminated by the ship's wake in the upper 10 m, we cannot resolve the role of wave-boundary layer dynamics on the vertical structure of dissipation. Since the wave forcing in September was weak, we do not expect a substantial contribution to the observed non-linear dependence of mixed-layer

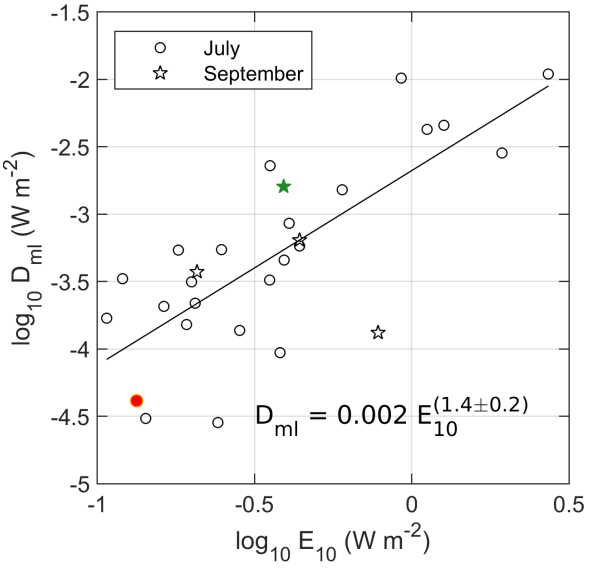

Figure 6. Depth-integrated dissipation rate in the mixed layer, D_{ml}, as a function of the wind energy input to the mixed layer, E_{10}. Stars and circles are data from the September and July cruises, respectively. The red circle is the data point from the RS2 process station where nonlinear internal waves were observed (Fer et al., 2020b). The green star is the data point at the process station at a front in September where convection was also important (Koenig et al., 2020). The black line is the regression line, with the equation indicated. The uncertainty is the 95% confidence interval.

dissipation on wind energy input. However the relatively large values of D_{ml} in July when E_{10} was large (circles in figure 6 might be associated with surface waves.

The front process station P (green star) is more energetic than what is expected from only wind forcing as convection is active on the warm side of the front ~~(green star)~~ (Koenig et al., 2020). Dissipation in the mixed layer at RS2 (~~orange~~ red circle) is only computed using the first casts as there is no data in the shallow mixed layer during the intense dissipation event driven by cross-slope tidal currents (Figure 3f). The presence of sea ice in the region can also explain the non-linearity of the relation between the wind energy and the energy dissipation in the mixed layer. Although the profiles were collected in ice-free conditions, some stations were close to the sea ice edge spotted from the ship.

5 ~~Mixing in the Atlantic Water layer~~

~~As the heat content in the Atlantic Water in the Arctic Ocean has the potential to melt the sea ice cover completely, it is important to quantify the turbulent dissipation rates and heat fluxes out of the Atlantic Water in present conditions of a warming Arctic. Depth-integrated dissipation rate from the base of the mixed layer to the Atlantic Water core is about 8.8×10^{-4} W m^{-2}, and the average dissipation rate is about 2×10^{-8} W kg^{-1}, almost as large as what is observed in the mixed layer (table 2). We~~

estimated the vertical turbulent heat flux between the upper limit of the Atlantic Water layer and the mixed layer depth (Figure 9a), in both summer and fall. Maximum positive heat flux (upward toward the surface) is observed near the 800 m isobath, reaching up to 30 W m^{-2} in July and 10 W m^{-2} in September. This isobath is representative of the average location of the core of Atlantic Water (Kolås et al., 2020). Outside the Atlantic Water boundary current, at about 20 km inshore and offshore from the 800 m isobath, vertical turbulent heat fluxes are negligible, with a maximum of 5 W m^{-2}. In July, the Atlantic Water core tends to be closer to the base of the mixed layer compared to September (Figure 9 a), implying that the heat contained in the Atlantic Water is more likely to reach the surface in July than in September. Meltwater in September enhances the stratification near the surface and isolates the Atlantic Water layer from the mixed layer. At some stations, vertical turbulent heat fluxes are negative (less than 5 W m^{-2}), directed downward from the surface toward the Atlantic Water layer. The negative fluxes are mainly found near the core of the Atlantic Water inflow. These negative heat fluxes are observed when warm water reaches the surface, and the temperature increases from the top of the Atlantic Water layer up to the surface. This situation is typical of summer conditions north of Svalbard where the Atlantic Water extends close to the surface and the cold halocline is absent (Polyakov et al., 2017).

The lateral (cross-isobath) distribution of the diapycnal heat fluxes is similar in July and September (Figure 9a). We therefore used all data points to fit a Gaussian curve (Figure 9b), with an aim to estimate the integrated heat loss from the Atlantic Water layer. Between -20 and +20 km, the heat loss due to vertical turbulent heat fluxes is about 1.2×10^5 W m^{-1} across the section. Using independent hydrographic observations but covering the same observational time period, Kolås et al. (2020) found that the average along-path change of heat content from section B to E was about 9.1×10^7 W m^{-1}, and about 9.6×10^6 W m^{-1} from section C to D, corresponding to an average heat loss of about 500 W m^{-2} north of Svalbard. Heat loss from the Atlantic Water layer by vertical turbulent heat fluxes to the upper ocean then accounts for only about 1% of the total Atlantic Water heat loss north of Svalbard. This estimate can be biased low since during the period of measurements wind forcing was weak to moderate with low variability. Processes that contribute to the turbulent heat loss of the Atlantic Water layer are discussed in section 7.

a) Lateral distribution of the mean vertical turbulent heat flux from the AW upper boundary to the base of the mixed layer. Horizontal axis is the horizontal distance to the 800 m isobath. Color code is the vertical distance between the upper boundary of the Atlantic Water layer and the mixed layer depth. Markers identify the stations collected in July (circles) and September (stars). b) A Gaussian fit (blue line) to the vertical turbulent heat flux from the Atlantic Water to the mixed layer depth (red crosses).

5 Tidal mixing

Previous observations show that north of Svalbard is a region of substantial tidal mixing (Rippeth et al., 2015; Fer et al., 2014). The location is northward of the critical latitude of the main diurnal and semi-diurnal semidiurnal tidal components (M_2 and K_1 and M_2). The critical latitude, also called the turning latitude, is where the tidal frequency matches the local inertial periodfrequency. The linear response at high latitudes is evanescent. The barotropic-to-baroclinic barotropic-to-baroclinic

energy conversion from the tidal activity results in trapped linear waves that can only propagate along topography guidelines, or nonlinear response with properties similar to lee waves (Vlasenko et al., 2003; Musgrave et al., 2016). A fraction of the energy in trapped waves or nonlinear waves will dissipate locally, leading to substantial vertical mixing (Padman and Dillon, 1991). In our observations, the dissipation rate below the mixed layer is typically low (table 2), but energetic turbulence observed at some locations (Figure 3) can be related to tidal forcing.

We select the profiles of turbulent heat fluxes and dissipation rates in categories of tidal current speed predicted from Arc5km 2018 at the time of the measurement. Tidal current speed is defined as large (> 5 cm s^{-1}) or low (< 5 cm s^{-1}) (Figure 7). The profiles in the corresponding categories are averaged with respect to height above bottom defined as the difference between the depth of the measurement and the seafloor depth. We obtained the average profiles as the maximum likelihood estimator from a lognormal distribution using the data points in 20 m vertical bins. The mixed layer was excluded in all the profiles to minimize the contribution from dissipation driven by surface processes.

From the seafloor to about 250 m height above bottom, dissipation rate was larger ($\epsilon > 10^{-8}$ W kg^{-1}) in conditions with strong tidal currents compared to weaker tidal currents ($\epsilon < 5 \times 10^{-9}$ W kg^{-1}). In both cases, the dissipation rate decreases quickly with height from the seafloor, down to dissipation rates of $\sim 5 \times 10^{-10}$ W kg^{-1} above 250 m from the bottom. Increase in dissipation rates for strong tidal forcing is associated with an absolute increase in the downward turbulent heat flux close to seafloor: -2.2 W m^{-2} when tidal currents were weak and about -3.2 W m^{-2} when tidal currents were strong.

Similar to the dissipation rate, the diapycnal diffusivity decreases with increasing height above bottom (Figure 7c). Based on the observations from north of Svalbard, we can deduce an empirical relation that would allow an estimate of the diffusivity in conditions of strong (> 5 cm s^{-1}) or weak (< 5 cm s^{-1}) tidal currents. Following St. Laurent et al. (2002), we use a functional form for the diffusivity expressed as:

$$\kappa = \kappa_{bg} + \kappa_{bot} \times e^{-h/z_{decay}}, \tag{5}$$

where κ_{bg} is a background diffusivity, κ_{bot} is the diffusivity value at the seafloor, h is the height above bottom and z_{decay} is the vertical decay scale of the diffusivity. We use ~~$\kappa_{bot} = 5 \times 10^{-5}$~~ $\kappa_{bg} = 5 \times 10^{-5}$ m^2 s^{-1}, based on observations. Fitted equations for large and low tidal current amplitude are shown above Figure 7c. With large tidal amplitudes, κ_{bot} approximately doubles and the decay scale increases from 18 to 22 m (95% confidence interval of 2 m).

We investigate the role of two distinct contributions from tidal currents to the turbulent mixing. While tidally-driven processes may lead to interior mixing away from the ~~sea bed~~ seabed (Fer et al., 2020b), bottom stress from barotropic tidal currents must be balanced by dissipation in bottom boundary layers. The tidal work can be representative of the barotropic-to-baroclinic conversion and can be related to the dissipation of propagating or trapped internal ~~waves dissipation and~~ wave energy, which can likely extend ~~farther~~ far into the water column. In the bottom boundary layer, the bottom stress from the barotropic tide also plays a role. The relative contributions to mixing through the tidal work and the tidally-driven bottom drag are unknown.

We analyse the vertically integrated dissipation rate in the bottom 250 m of the water column D_{250} (and below the surface mixed layer) separately with respect to tidal work and the tidally-driven bottom drag (Figure 8). ~~Following Nash et al. (2006),~~

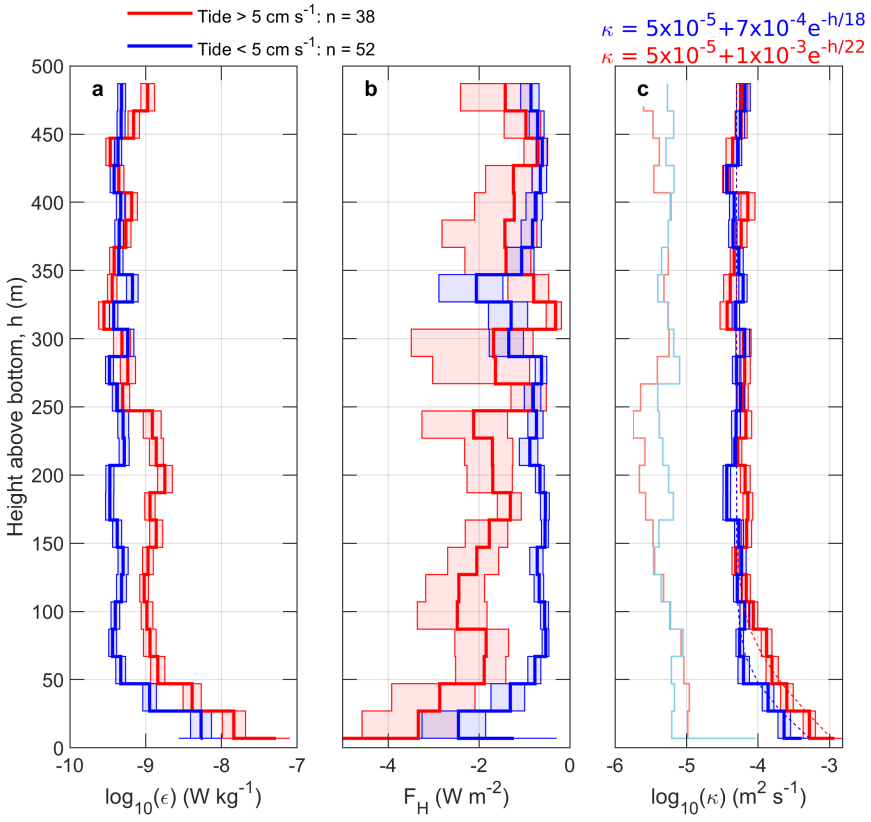

Figure 7. Average profiles of a) dissipation rate ϵ, b) turbulent heat flux F_H and c) diapycnal diffusivity κ for small (blue) and large (red) tidal current amplitudes estimated from Arc5km2018 at the time and location of each station. Average profiles are obtained as the maximum likelihood estimator from a lognormal distribution using the data points in 20 m vertical bins. The vertical axis is height above bottom, relative to the seafloor depth from the echo sounder. n indicates the number of batch-averaged profiles for each tidal forcing category. Thin lines in (c) are the corresponding profiles for diffusivity at the lowest detection level (obtained by imposing a noise level for dissipation rate of 1×10^{-10} W kg^{-1}). The dashed lines are the curve fits using an exponential function. Resulting equations with the best fit coefficients are shown above the panel. The shading is the 95% confidence envelope of the maximum likelihood.

~~the~~ The total rate of work by barotropic tidal currents interacting with topography ~~is~~ was computed as the product of the Baines force (Baines, 1982) ~~, $F_{Baines} = N^2 w \omega^{-1}$,~~ and the barotropically induced vertical velocity following Nash et al. (2006), for the main diurnal and semidiurnal constituents. D_{250} does not correlate well with the tidal work, ~~$w = \mathbf{u} \cdot \nabla \mathbf{H}(z/H)$, where ω is the tidal wave frequency, $N(z)$ is the Brunt Väisäläfrequency, $\mathbf{u}$ is the tidal current vector and $\nabla \mathbf{H}$ is the bottom slope vector. Excluding the wave frequency as a variable, we introduce the following parameter related to tidal work:~~

$W_{tidal} = N^2|\mathbf{u} \cdot \nabla \mathbf{H}|^2$.

W_{tidal}, at the time of observations (not shown). A least-squares power-law fit results in an uncertainty on the power which is more than 50% of its estimated value: $D_{250} = 7 \times 10^{-3} W_{tidal}^{0.16 \pm 0.09}$

~~where N is the Brunt Väisäläfrequency near bottom (averaged in the 100 m height above bottom).~~ The tidally-driven bottom drag is examined next, expressed as in Jayne and St. Laurent (2001):

$$W_{botdrag} = \rho_0 C_d |\mathbf{u}|^3, \tag{6}$$

where C_d is the bottom drag coefficient, ρ_0 is the seawater density and $\mathbf{u}$ is the tidal current vector.

~~In both equations,~~ Note that this equation is analogous to the drag relation for the wind energy flux E_{10} (in section 4.2). In calculations two different tidal currents are used: the instantaneous tidal speed u_t at the time and location of each station and a statistical estimate of the representative cross-isobath tidal current, u_{rms}, at the location of each station (Figure 8). Both are obtained from the Arc5km2018 model. We calculated u_{rms} from the predicted local cross-isobath component of the tidal currents over an arbitrary 30-day window using all constituents; this choice offers a parameter easily available for parameterization purposes, independent of observations.

In analyzing the vertically integrated dissipation rates with respect to local forcing at the time of observations (Figures 8a~~, e~~), we averaged the process stations in batches as explained in section 3; this allows for including some time variability in the observations. For the analysis of typical tidal forcing (not time variable), we averaged each process station as one data point because each location is associated with a time independent u_{rms} (Figure 8b~~, d). D_{250} does not correlate well with the tidal work-related parameter at the time of observations (figures 8a). A least-squares power-law fit results in an uncertainty on the power which is more than 30% of its estimated value.~~). The local bottom drag at the time of observations correlates ~~somewhat better~~ well with D_{250}, and follows the power-law fit with a considerable scatter (uncertainty on the power is ~~reduced to~~ less than 25% its estimated value, figures 8~~c). a~~). This nonlinear relationship between D_{250} (dissipation in the bottom 250 m) and $W_{botdrag}$ shows parallels with the nonlinear relationship between D_{ml} (dissipation in the surface mixed layer) and E_{10}. If we force a linear relation in panel ~~c~~a, we find a drag coefficient of $C_d = 8.2 \times 10^{-4}$.This value is ~~of the same order of magnitude as the one~~ comparable to but smaller than the typical range of bottom drag values of $(1-3) \times 10^{-3}$ and the bottom drag deduced from in situ observations in ~~the~~ Bering Strait: 2.3×10^{-3} (Couto et al., 2020). The red data points in figure 8 are from the station RS2, where ~~large mixing~~ energetic turbulence was observed from dissipation of ~~non-linear~~ nonlinear internal waves (Fer et al., 2020b). It partly explains why larger dissipation rates are observed here than what could be expected from the tidally-driven bottom drag alone. The analysis is repeated using the ~~tidal work and~~ bottom drag parameters calculated using the typical cross-isobath tidal forcing u_{rms} (Figure 8b~~and d~~). The scatter is reduced, and particularly, the bottom-drag relation offers a useful parameterization to infer vertically-integrated dissipation rates. ~~A pan-Arctic coarse estimate~~ An estimate along the margin of the Eurasian basin will be given in the ~~following section~~ discussion using the relation in Figure 8~~d~~b.

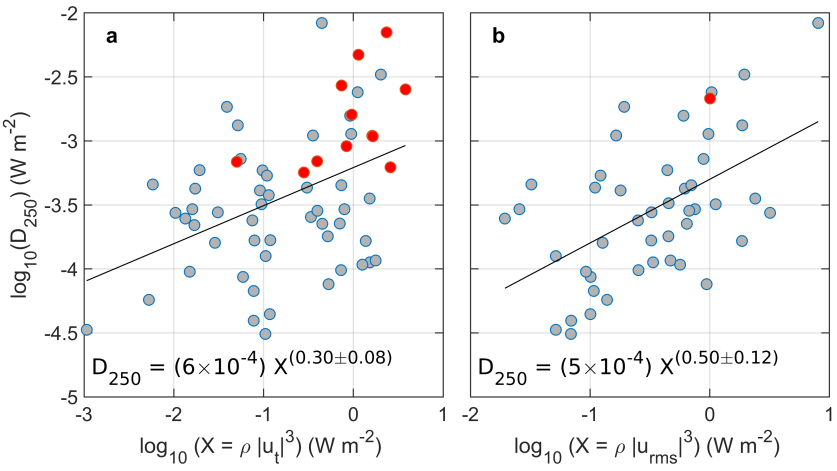

Figure 8. Depth-integrated dissipation rate in the bottom 250 m (D_{250}) regressed against a) the instantaneous ~~(using u_t) values of a tidal-work related parameter, b) the statistically representative (using u_{rms}) typical values of the same parameter, c) the instantaneous~~ tidally-driven bottom drag, and ~~d~~b) the typical tidally-driven bottom drag (using u_{rms}). See text for details. Linear fits on logarithmic parameter space (i.e., power-law fits) are the black lines and the corresponding equations are indicated with the 95% confidence levels. Red dots are the data points from the RS2 station. Process stations are batch-averaged (in sets of 4-5 consecutive profiles) in ~~panels~~ panel a~~and c~~, and averaged over the station duration in ~~panels~~ panel b~~and d~~.

6 Mixing in the Atlantic Water layer

As the heat content in the Atlantic Water in the Arctic Ocean has the potential to melt the sea ice cover completely, it is important to quantify the turbulent dissipation rates and heat fluxes out of the Atlantic Water in the new conditions of a warming Arctic. Depth-integrated dissipation rate from the base of the mixed layer to the Atlantic Water core is about 8.8×10^{-4} W m^{-2}, and the average dissipation rate is about 2×10^{-8} W kg^{-1}, almost as large as what is observed in the mixed layer (table 2). We estimated the vertical turbulent heat flux between the upper limit of the Atlantic Water layer and the mixed layer depth (Figure 9a), in both summer and fall. Maximum positive heat flux (upward toward the surface) is observed near the 800 m isobath, reaching up to 30 W m^{-2} in July and 10 W m^{-2} in September. This isobath is representative of the average location of the core of Atlantic Water (Kolås et al., 2020). Outside the Atlantic Water boundary current, at about 20 km inshore and offshore from the 800 m isobath, vertical turbulent heat fluxes are negligible, with a maximum of 5 W m^{-2}. In July, the Atlantic Water core tends to be closer to the base of the mixed layer compared to September (Figure 9 a), implying that the heat contained in the Atlantic Water is more likely to reach the surface in July than in September. Meltwater in September enhances the stratification near the surface and isolates the Atlantic Water layer from the mixed layer. At some stations, vertical turbulent heat fluxes are negative (0 to -5 W m^{-2}), directed downward from the surface toward the Atlantic Water layer. The negative fluxes are mainly found near the core of the Atlantic Water inflow. These negative heat fluxes are observed when warm water reaches the surface, and the temperature increases from the top of the Atlantic Water layer up to the surface. This situation is typical

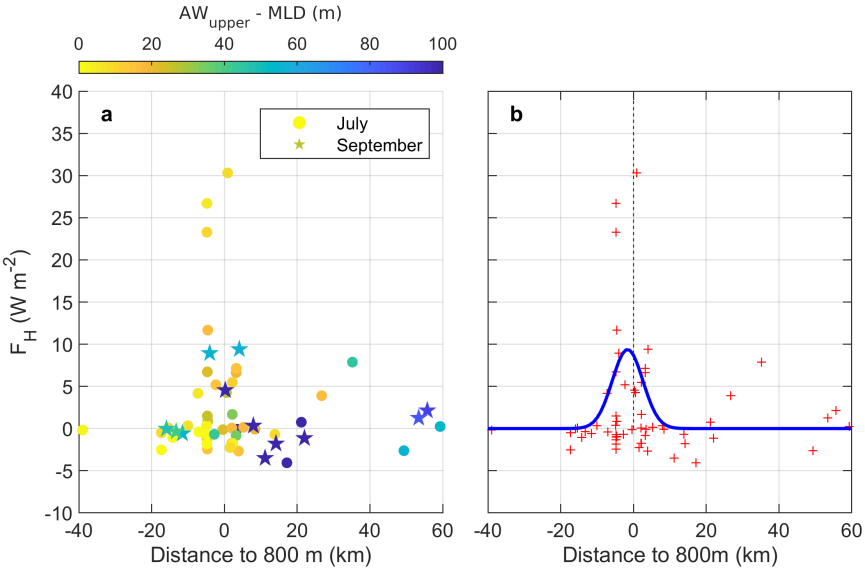

Figure 9. a) Lateral distribution of the mean vertical turbulent heat flux from the AW upper boundary to the base of the mixed layer. Horizontal axis is the horizontal distance to the 800 m isobath. Color code is the vertical distance between the upper boundary of the Atlantic Water layer and the mixed layer depth. Markers identify the stations collected in July (circles) and September (stars). b) A Gaussian fit (blue line) to the vertical turbulent heat flux from the Atlantic Water to the mixed layer depth (red crosses).

of summer conditions north of Svalbard where the Atlantic Water extends close to the surface and the cold halocline is absent (Polyakov et al., 2017).

The lateral (cross-isobath) distribution of the diapycnal heat fluxes is similar in July and September (Figure 9a). We therefore used all data points to fit a Gaussian curve (Figure 9b), with an aim to estimate the integrated heat loss from the Atlantic Water layer. Between -20 and +20 km, the heat loss due to vertical turbulent heat fluxes is about 1.2×10^5 W m^{-1}. Using independent hydrographic observations but covering the same observational time period, Kolås et al. (2020) found that the average along-path change of heat content from section B to E was about 9.1×10^7 W m^{-1}, and about 9.6×10^6 W m^{-1} from section C to D, corresponding to an average heat loss of about 500 W m^{-2} north of Svalbard. Heat loss from the Atlantic Water layer by vertical turbulent heat fluxes to the upper ocean then accounts for only about 1% of the total Atlantic Water heat loss north of Svalbard. This estimate can be biased low since during the period of measurements wind forcing was weak to moderate with low variability. Processes that contribute to the turbulent heat loss of the Atlantic Water layer are discussed in section 7.

7 Discussion

7.1 ~~Pan-Arctic estimates~~ Estimates of tidally-driven dissipation ~~rates~~rate in the Eurasian Basin

Turbulent mixing in the Arctic is not well-documented, and measurements close to the bottom are scarce. The bottom drag estimated from the Arc5km2018 predictions in the Arctic Ocean, using a constant drag coefficient, is larger on the shelf and on the ridges than in the deep basin (not shown), as a result of sensitivity to the strength of barotropic tidal current. These areas coincide with regions of enhanced tidal activity in the Arctic (Padman and Erofeeva, 2004). Using this tidally-driven bottom drag and the relation inferred from the data collected north of Svalbard (section ~~5.3~~ 5 and equation in Figure 8~~d~~b), we estimate the depth-integrated dissipation rate. The highest bottom depth-integrated dissipation rates in the Arctic are found on the shelves, and are consistent with the pan-Arctic observations compiled and presented in Rippeth et al. (2015), reaching 10^{-3} W m^{-2} (not shown).

Because the parameterization is obtained using a limited data set from a localized region north of Svalbard, instead of presenting Arctic-wide maps we concentrate on the Eurasian Basin from north of Svalbard into the East Siberian Sea. The cross-isobath tidal currents along this transect, particularly in the Laptev Sea, are strong (see Fig. 1 of Fer et al. (2020b)). Figure 10 shows the time-averaged cross-isobath tidal current amplitude~~and the 250 m bottom~~ , and the depth-integrated dissipation rate in the bottom 250 m estimated using the equation in Figure 8~~d~~ b, along the continental slope of the Eurasian basin. The largest tidal speeds are observed north of Svalbard and in the eastern part of the Laptev Sea where the slope connects to the Lomonosov Ridge, reaching more than 0.1 m s^{-1} (Figure 10a). The largest average bottom dissipation rates across the continental slope are observed at 35°E, just east of Svalbard and at the Lomonosov Ridge, reaching 3.2×10^{-4} W m^{-2}. We present two estimates for the dissipation: vertically-integrated dissipation rate in the bottom 250 m, D_{250}, averaged laterally between the 400 m and 1200 m isobaths (blue line and left axis, Figure 10b), and D_{250} integrated meridionally between the 400 m and 1200 m ~~,~~ isobaths (red line and right axis, Figure 10b). This volume-integrated dissipation rate, per unit metre along the shelf break, shows variations similar to the averaged D_{250}, except at 70°E. This is the location of the Santa Anna Trough, where the Atlantic Water from the Barents Sea flows into the Arctic Ocean and where the distance between the 400 and 1200 m isobaths triples compared to the rest of the Eurasian continental slope. Rippeth et al. (2015) argued, based on microstructure measurements and tidal velocities from the TPXO8 inverse solution that the energy supporting much of the enhanced dissipation along the continental slopes in the Eurasian Basin, and more specifically north of Svalbard and around the Lomonosov Ridge, is of tidal origin. The mean-integrated dissipation over the Atlantic layer observed in Rippeth et al. (2015) is of similar order of magnitude as the depth-integrated dissipation in the bottom 250 m deduced from the tidally-driven bottom drag as observed in our study. However, the bottom depth-integrated dissipation rate extrapolated from a local relation valid north of Svalbard to the Arctic Ocean must be considered with caution.

As the Eurasian Arctic is poleward of the critical latitude for most of the main tidal constituents, the response to tidal flow over sloping topography can be nonlinear when the topographic obstruction of the stratified flow is large. Legg and Klymak (2008) proposed that an inverse Froude number, Fr_ω^{-1}, based on a vertical excursion distance of the tidal current over bottom slope, can be used to estimate the possibility of occurrence of highly nonlinear jump-like lee waves, such as those observed at

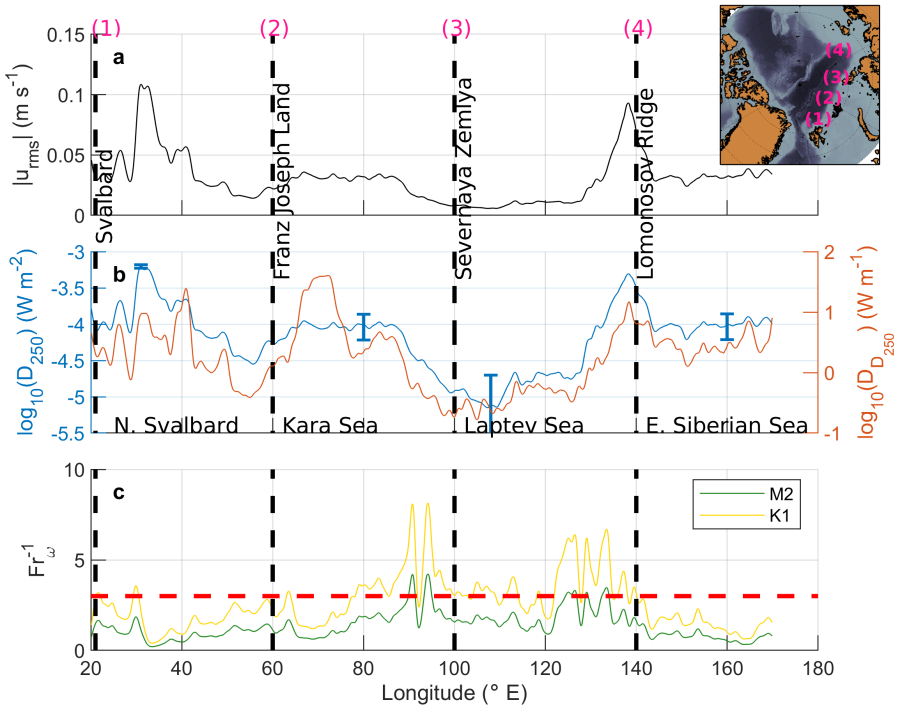

Figure 10. a) Typical cross-isobath tidal speed along the Eurasian continental slope obtained from Arc5km2018 and averaged meridionally between the 400 m and 1200 m isobaths b) left axis: the depth-integrated dissipation rate in the bottom 250 m, D_{250}, calculated from the tidally-driven bottom drag using the relation in Figure 8~~d~~b, averaged between the 400 m and 1200 m isobaths. The blue vertical bars, shown at selected locations for clarity, are the error bars from the uncertainty on the equation in Figure 8~~d~~b. Right axis: D_{250} integrated laterally between the 400 m and 1200 m isobaths. c) Inverse Froude number for both the ~~semi-diurnal~~ semidiurnal M_2 (green) and the diurnal K_1 tidal components (yellow). The red dashed line is $Fr_\omega^{-1} = 3$, a threshold for the development of nonlinear processes (Legg and Klymak, 2008).

station RS2 (Fer et al., 2020b) or modelled over the Spitsbergen Bank (Rippeth et al., 2017), a shallow bank south of Svalbard and poleward of the M_2 critical latitude. The inverse Froude number is expressed as:

$$Fr_\omega^{-1} = \frac{|\nabla \mathbf{H}| N}{\omega} \tag{7}$$

where $|\nabla \mathbf{H}|$ is the bottom slope and ω is the tidal frequency. In our calculations we used the Brunt Väisälä frequency N near the bottom, extracted from the MIMOC climatology in August (the result is not sensitive to this choice as the near bottom stratification does not have a strong seasonal cycle). When $Fr_\omega^{-1} > 3$, the vertical excursion distance induced by tidal currents is sufficiently large that hydraulic jumps could occur and nonlinear waves can develop (Legg and Klymak, 2008). The calculations along the Eurasian shelf break are presented in figure 10c for the semidiurnal and the diurnal tidal forcing. Along the Eurasian slope, we expect nonlinear internal waves to develop for the diurnal tidal forcing in the eastern part of the Kara

and Laptev Seas, where Fr_ω^{-1} is much larger than 3, the threshold value for the development of nonlinear processes. Values slightly above this threshold are also ~~seen~~ observed north of Svalbard~~, consistent with the~~. In the region north of Svalbard and in the eastern part of the Laptev Sea, the large depth-integrated dissipation rate observed in Figure 10b can be driven by nonlinear waves implied by the peaks of Fr_ω^{-1} (figure 10c). These two areas warrant further studies. In the eastern part of the Kara Sea, however, the depth-integrated dissipation rates are relatively low despite the large inverse Froude number values that suggest nonlinear processes could develop there.

North of Svalbard, observations of nonlinear internal waves was documented in Fer et al. (2020b) during the July cruise at RS2. They showed abrupt isopycnal vertical displacements of 10–50 m and an intense dissipation associated with cross-isobath diurnal tidal currents of ~ 0.15 m s^{-1}. The dissipation of these nonlinear internal waves creates an increase in dissipation in the whole water column by a factor of 100 and turbulent heat fluxes are about 15 W m^{-2} compared with the background turbulent heat flux of 1 W m^{-2} (Fer et al., 2020b). The increase in dissipation rate driven by these nonlinear waves is also noticeable in Figure 8a and c (the red dots). At this location, the inverse Froude number for the diurnal frequency exceeds 3, supporting the interpretation that such conditions can favor the development of nonlinear processes.

7.2 ~~Impact of the melt water on the near-surface mixing~~

~~The observations used in this study indicate that although dissipation rates at the base of the mixed layer are similar from summer to fall, the downward buoyancy and upward salinity fluxes are larger in September due to an increase in the meltwater content.~~

~~In the future, sea ice meltwater is expected to increase and turbulent mixing near the surface to decrease. But at the same time, the increase in melt water is associated with a decrease in the sea ice cover, hence a possible increase in the momentum transfer from the wind into the ocean and a possible increase in turbulence (Dosser and Rainville, 2016). The balance between these two trends, increase in sea ice melt and increase in the open ocean area, with opposite effect on the turbulent mixing was tentatively addressed looking at a 1D model in Davis et al. (2016). They found that in the Eurasian Basin within a decade an elevated shear will deepen the halocline and strengthen the stratification over the Atlantic Water thermocline, thus reducing the vertical heat flux. But in a long-term perspective, the mixed layer begins to cool and the sea ice cover can only be significantly affected if the elevated mixing is sufficient to erode the stratification barrier associated with the cold halocline. Using a steady-state vertical advection-diffusion balance and an exponential fit to the salinity and density profiles from an annual climatology, Fer (2009) estimated that a basin-averaged diffusivity larger than 5×10^{-5} m^2 s^{-1} would erode and eventually remove the steady-state cold halocline layer.~~

~~Several studies also suggest that the meltwater will also have consequences on the nitrates fluxes (Randelhoff et al., 2017). Randelhoff et al. (2016) found that Atlantic Water heat leads to stronger melt rates north of Svalbard and an earlier onset of stratification which might be indirectly linked to bloom development.~~

7.2 Atlantic Water heat loss

The Atlantic Water looses heat as it propagates cyclonically along the continental slope in the Arctic Ocean. Around the Yermak Plateau, the along-path cooling and freshening are estimated to be $0.2°C$ per 100 km and 0.01 g kg^{-1} per 100 km, corresponding to a surface heat flux between 400 and 500 W m^{-2} (Boyd and D'Asaro, 1994; Cokelet et al., 2008; Kolås and Fer, 2018). We found that the upward heat loss from turbulent heat fluxes from the Atlantic Water layer up to the mixed layer reached on average 8 W m^{-2}. This figure is one order of magnitude larger than vertical heat flux from the Atlantic Water to the surface in the Laptev Sea (on the order of 0.1 - 1 W m^{-2}, Polyakov et al. (2019)). North of Svalbard and in the Laptev Sea, heat loss due to turbulent vertical mixing represents less than 10% of the total heat loss of the Atlantic Water (Kolås et al., 2020; Polyakov et al., 2019).

~~Vertical turbulent heat fluxes are not the main source of cooling of the Atlantic Water layer in the Arctic. Ivanov and Timokhov (2019) rev~~ Ivanov and Timokhov (2019) estimated that from the Yermak Plateau to the Lomonosov ~~ridge~~Ridge, 41% of the Atlantic Water heat is lost to ~~the~~ atmosphere, 31% to ~~the~~ deep ocean and 20% is lost laterally.

Heat loss resulting from vertical heat fluxes contributes to the heat loss to atmosphere and to deep ocean, but not to the lateral heat loss. Several processes can lead to lateral heat loss North of Svalbard, ~~a particular sink for the Atlantic Water heat content is~~ including eddy spreading from the slope into the basin (Crews et al., 2018; Våge et al., 2016). Using eddy-resolving regional model results, Crews et al. (2018) found that eddies export 1.0 TW out of the boundary current, delivering heat into the interior Arctic Ocean at an average rate of ~ 15 W m^{-2}. ~~Large heat losses during extreme events should not be ignored. For example, Meyer et al. (2017) found that at steady state, heat fluxes across the 0°C isotherm are about 7 W m^{-2}; however, turbulent heat fluxes during storms can exceed 30 W m^{-2}.~~ West of Svalbard, Kolås and Fer (2018) found that the measured turbulent heat flux in the WSC ~~is~~ was too small to account for ~~its cooling rate~~ the cooling rate of the Atlantic Water layer, but reported substantial contribution from energetic convective mixing of an unstable bottom boundary layer on the slope. Convection was driven by Ekman advection of buoyant water across the slope, and complements the turbulent mixing in the cooling process. The estimated lateral buoyancy flux ~~is~~ was about 10^{-8} W kg^{-1} (Kolås and Fer, 2018), sufficient to maintain a large fraction of the observed dissipation rates, and corresponds to a heat flux of approximately 40 W m^{-2}. ~~Although this process is documented west of Svalbard, we~~ We can expect similar processes to ~~occur north of Svalbard and~~ extract heat and salt from the Atlantic Water core north of Svalbard. Such processes can explain why turbulent heat fluxes are only responsible for 10% of the Atlantic heat loss north of Svalbard. Furthermore, large heat loss during extreme events should not be ignored. For example, Meyer et al. (2017) found that the average heat flux of about 7 W m^{-2} across the 0°C isotherm increased during storms, exceeding 30 W m^{-2}. During our survey without extreme wind events, the turbulent heat fluxes represent only a small portion of the heat loss of the Atlantic Water.

8 Summary

We reported on observations of turbulence north of Svalbard, collected during two cruises in summer and fall 2018, in conditions with varying tidal forcing and weak to moderate wind forcing with low variability. We describe the observed structure

of dissipation rates and vertical mixing in the region and identify the main processing supplying energy for turbulence. This dataset complements the scarce observations and offers further insight to turbulent mixing processes in the Arctic Ocean.

During the observation period, from July to September, the surface meltwater content increases. Averaged across the base of the mixed layer, salt and buoyancy fluxes more than double from summer to fall, although the vertically-integrated dissipation rate in the mixed layer (D_{ml}) remains similar. Variability of the turbulent dissipation in the mixed layer varies nonlinearly with the energy input from the wind E_{10}, approximated by $D_{ml} \propto E_{10}^{1.4}$. The scatter is large, however, from turbulence produced in the mixed layer by other processes such as convection.

In the deeper part of the water column, tidal forcing appears to be one of the main sources of mixing. When the tidal current amplitude exceeds 5 cm s^{-1}, near-bottom dissipation rates and diapycnal diffusivity double. The vertical decay scale of the diffusivity is 22 m for those strong tidal currents, compared to 18 m for weaker tidal currents; the bottom diffusivity is larger with strong tidal currents than for weaker ones (1×10^{-3} m^2 s^{-1} and 7×10^{-4} m^2 s^{-1}, respectively). The variability of the vertically-integrated dissipation rate in the bottommost 250 m, D_{250}, can be approximated by bottom stress from the barotropic tidal current, parameterized using a quadratic bottom drag. Using ~~the cross-isobath component of the tidal currents predicted over 30 days from Arc5km2018~~a statistical estimate of the typical cross-isobath tidal currents, regression of D_{250} against the tidally-driven bottom drag $W_{botdrag}$ gives $D_{250} \propto W_{botdrag}^{0.50}$. The average bottom drag coefficient north of Svalbard is estimated to be about 8×10^{-4}. Applying the power-law fit to tidal currents along the Eurasian continental slope, we find that turbulence is enhanced north of Svalbard and east of the Laptev Sea above the Lomonosov ridge, with D_{250} reaching 3.4×10^{-4} W m^{-2}. Higher above the seafloor, the dissipation rates can also increase as a result of breaking nonlinear internal waves driven by tidal currents. A Froude number based calculation suggests that nonlinear response and internal hydraulic jumps are expected to develop north of Svalbard, in the Kara and Laptev Seas. The generalisation of our results to the Eurasian Basin should however be considered with caution as it is based on an empirical relation extrapolated from north of Svalbard. More in situ observations from different sites in the Eurasian Basin and elsewhere in the Arctic are needed to confirm our results.

The Atlantic Water layer north of Svalbard cools and freshens by mixing with the surrounding waters. ~~Heat~~ Across the warm Atlantic Water boundary current, heat loss due to vertical turbulent ~~heat~~ fluxes from the top of the Atlantic Water layer to the mixed layer is the largest above the 800 m isobath, reaching ~ 30 W m^{-2}, ~~above the 800 m isobath,~~ corresponding to the location of the ~~Atlantic Water~~ boundary current core. In our dataset, the average heat loss from the Atlantic Water layer due to vertical mixing is about 5 W m^{-2} and accounts for only about 1% of the estimated total heat loss of the Atlantic Water layer. ~~Although the vertical turbulent heat fluxes are expected to increase during storms , more~~ Increased vertical mixing during storms would add to this figure. However, integrated studies addressing lateral mixing processes, frontal systems as well as ~~vertical mixing~~ extreme conditions such as storms are needed to close the heat budget in this region.

Data availability. All data are available from the Norwegian Marine Data Centre; data sets from the July cruise (KB 2018616) are available at https://doi.org/10.21335/NMDC-2047975397, data sets from the September cruise (KH 2018709) are available at https://doi.org/10.21335/NMDC-2039932526.

Author contributions. ZK drafted the manuscript. All the authors collected, processed and analyzed the observations, edited and commented on the manuscript.

Competing interests. Ilker Fer is a member of the editorial board of Ocean Science, but other than that the authors declare no competing interests.

Acknowledgements. This work was supported by the Nansen Legacy Project, project number 27272. We thank the officers, crew and scientists of the *R/V Kronprins Haakon* cruise in September 2018 and of the *R/V Kristine Bonnevie* cruise in July 2018.

References

Årthun, M., Eldevik, T., Smedsrud, L., Skagseth, Ø., and Ingvaldsen, R.: Quantifying the influence of Atlantic heat on Barents Sea ice variability and retreat, Journal of Climate, 25, 4736–4743, https://doi.org/10.1175/JCLI-D-11-00466.1, 2012.

Baines, P. G.: On internal tide generation models, Deep Sea Research Part A. Oceanographic Research Papers, 29, 307–338, https://doi.org/10.1016/0198-0149(82)90098-X, 1982.

Bouffard, D. and Boegman, L.: A diapycnal diffusivity model for stratified environmental flows, Dynamics of Atmospheres and Oceans, 61, 14–34, https://doi.org/10.1016/j.dynatmoce.2013.02.002, 2013.

Boyd, T. J. and D'Asaro, E. A.: Cooling of the West Spitsbergen Current: Wintertime observations west of Svalbard, J. Geophys. Res., 99, 22,597–22,618, https://doi.org/10.1029/94JC01824, 1994.

Cokelet, E. D., Tervalon, N., and Bellingham, J. G.: Hydrography of the West Spitsbergen Current, Svalbard Branch: Autumn 2001, J. Geophys. Res., 113, C01006, https://doi.org/10.1029/2007JC004150, 2008.

Couto, N., Alford, M. H., MacKinnon, J., and Mickett, J. B.: Mixing rates and bottom drag in Bering Strait, Journal of Physical Oceanography, 50, 809–825, https://doi.org/10.1175/JPO-D-19-0154.1, 2020.

Crews, L., Sundfjord, A., Albretsen, J., and Hattermann, T.: Mesoscale Eddy Activity and Transport in the Atlantic Water Inflow Region North of Svalbard, J. Geophys. Res., 123, 201–215, https://doi.org/10.1002/2017JC013198, 2018.

Crews, L., Sundfjord, A., and Hattermann, T.: How the Yermak Pass Branch Regulates Atlantic Water Inflow to the Arctic Ocean, Journal of Geophysical Research: Oceans, 124, 267–280, https://doi.org/10.1029/2018JC014476, 2019.

Davis, P. E., Lique, C., Johnson, H. L., and Guthrie, J. D.: Competing effects of elevated vertical mixing and increased freshwater input on the stratification and sea ice cover in a changing Arctic Ocean, Journal of Physical Oceanography, 46, 1531–1553, https://doi.org/10.1175/JPO-D-15-0174.1, 2016.

Dosser, H. V. and Rainville, L.: Dynamics of the changing near-inertial internal wave field in the Arctic Ocean, J. Phys. Oceanogr., 46, 395–415, https://doi.org/10.1175/jpo-d-15-0056.1, 2016.

Duarte, P., Sundfjord, A., Meyer, A., Hudson, S. R., Spreen, G., and Smedsrud, L. H.: Warm Atlantic water explains observed sea ice melt rates north of Svalbard, Journal of Geophysical Research: Oceans, 125, e2019JC015 662, https://doi.org/10.1029/2019JC0156622, 2020.

Erofeeva, S. and Egbert, G.: Arc5km2018: Arctic Ocean Inverse Tide Model on a 5 kilometer grid, 2018. Dataset., https://doi.org/10.18739/A21R6N14K, 2020.

Fer, I.: Weak vertical diffusion allows maintenance of cold halocline in the central Arctic, Atmospheric and Oceanic Science Letters, 2, 148–152, https://doi.org/10.1080/16742834.2009.11446789, 2009.

Fer, I., Müller, M., and Peterson, A. K.: Tidal forcing, energetics, and mixing near the Yermak Plateau, Ocean Science Discussions, 11, https://doi.org/doi:10.5194/os-11-287-2015, 2014.

Fer, I., Koenig, Z., Kolås, E., Falck, E., Fossum, T., Ludvigsen, M., Marnela, M., Nilsen, F., Norgren, P., and Skogseth, R.: Physical oceanography data from the cruise KH 2018709 with R.V. Kronprins Haakon, 12-24 September 2018, Data Set, https://doi.org/10.21335/NMDC-2039932526, 2019.

Fer, I., Koenig, Z., Bosse, A., Falck, E., Kolås, E., and Nilsen, F.: Physical oceanography data from the cruise KB 2018616 with R.V. Kristine Bonnevie., Data Set, https://doi.org/10.21335/NMDC-2047975397, 2020a.

Fer, I., Koenig, Z., Kozlov, I. E., Ostrowski, M., Rippeth, T. P., Padman, L., Bosse, A., and Kolås, E.: Tidally forced lee waves drive turbulent mixing along the Arctic Ocean margins, Geophysical Research Letters, 47, e2020GL088 083, https://doi.org/10.1029/2020GL088083, 2020b.

Gregg, M., D'Asaro, E., Riley, J., and Kunze, E.: Mixing efficiency in the ocean, Annual review of marine science, 10, 443–473, https://doi.org/10.1146/annurev-marine-121916-063643, 2018.

Guarino, M.-V., Sime, L. C., Schröeder, D., Malmierca-Vallet, I., Rosenblum, E., Ringer, M., Ridley, J., Feltham, D., Bitz, C., Steig, E. J., et al.: Sea-ice-free Arctic during the Last Interglacial supports fast future loss, Nature Climate Change, pp. 1–5, https://doi.org/10.1038/s41558-020-0865-2, 2020.

Ivanov, V. and Timokhov, L.: Atlantic Water in the Arctic Circulation Transpolar System, Russian Meteorology and Hydrology, 44, 238–249, https://doi.org/10.3103/S1068373919040034, 2019.

Ivanov, V., Alexeev, V., Koldunov, N. V., Repina, I., Sandø, A. B., Smedsrud, L. H., and Smirnov, A.: Arctic Ocean heat impact on regional ice decay: A suggested positive feedback, Journal of Physical Oceanography, 46, 1437–1456, https://doi.org/10.1175/JPO-D-15-0144.1, 2016.

Jakobsson, M., Mayer, L., Coakley, B., Dowdeswell, J. A., Forbes, S., Fridman, B., Hodnesdal, H., Noormets, R., Pedersen, R., Rebesco, M., Schenke, H. W., Zarayskaya, Y., Accettella, D., Armstrong, A., Anderson, R. M., Bienhoff, P., Camerlenghi, A., Church, I., Edwards, M., Gardner, J. V., Hall, J. K., Hell, B., Hestvik, O., Kristoffersen, Y., Marcussen, C., Mohammad, R., Mosher, D., Nghiem, S. V., Pedrosa, M. T., Travaglini, P. G., and Weatherall, P.: The International Bathymetric Chart of the Arctic Ocean (IBCAO) Version 3.0, Geophys. Res. Lett., 39, L12609, https://doi.org/10.1029/2012gl052219, 2012.

Jayne, S. and St. Laurent, L.: Parameterizing tidal dissipation over rough topography, Geophys. Res. Lett., 28, 811–814, https://doi.org/10.1029/2000GL012044, 2001.

Koenig, Z., Provost, C., Sennechael, N., Garric, G., and Gascard, J.-C.: The Yermak Pass Branch: A Major Pathway for the Atlantic Water North of Svalbard?, J. Geophys. Res., https://doi.org/10.1002/2017JC013271, 2017.

Koenig, Z., Fer, I., Kolås, E., Fossum, T., Norgren, P., and Ludvigsen, M.: Observations of turbulence at a near-surface temperature front in the Arctic Ocean, J. Geophys. Res. Oceans, https://doi.org/10.1029/2019JC015526, 2020.

Kolås, E. and Fer, I.: Hydrography, transport and mixing of the West Spitsbergen Current: the Svalbard Branch in summer 2015, Ocean Sci., 14, 1603–1618, https://doi.org/10.5194/os-14-1603-2018, 2018.

Kolås, E. H., Koenig, Z., Fer, I., Nilsen, F., and Marnela, M.: Structure and transport of Atlantic Water north of Svalbard from observations in summer and fall 2018, Journal of Geophysical Research: Oceans, 125, e2020JC016 174, https://doi.org/10.1029/2020JC016174, 2020.

Krishfield, R. A. and Perovich, D. K.: Spatial and temporal variability of oceanic heat flux to the Arctic ice pack, J. Geophys. Res., 110, C07 021, https://doi.org/10.1029/2004JC002293, 2005.

Large, W. and Pond, S.: Open ocean momentum flux measurements in moderate to strong winds, Journal of Physical Oceanography, 11, 324–336, https://doi.org/10.1175/1520-0485(1981)011<0324:OOMFMI>2.0.CO;2, 1981.

Legg, S. and Klymak, J.: Internal hydraulic jumps and overturning generated by tidal flow over a tall steep ridge, Journal of Physical Oceanography, 38, 1949–1964, https://doi.org/10.1175/2008JPO3777.1, 2008.

Lenn, Y.-D., Rippeth, T. P., Old, C. P., Bacon, S., Polyakov, I., Ivanov, V., and Hölemann, J.: Intermittent Intense turbulent mixing under Ice in the Laptev Sea continental shelf, J. Phys. Oceanogr., 41, 531–547, https://doi.org/10.1175/2010JPO4425.1, 2011.

Lincoln, B. J., Rippeth, T. P., Lenn, Y.-D., Timmermans, M. L., Williams, W. J., and Bacon, S.: Wind-driven mixing at intermediate depths in an ice-free Arctic Ocean, Geophys. Res. Lett., 43, 9749–9756, https://doi.org/https://doi.org/10.1002/2016GL070454, 2016.

Løken, T. K., Rabault, J., Jensen, A., Sutherland, G., Christensen, K. H., and Müller, M.: Wave measurements from ship mounted sensors in the Arctic marginal ice zone, arXiv preprint arXiv:1911.07612, 2019.

Maykut, G. A. and McPhee, M. G.: Solar heating of the Arctic mixed layer, J. Geophys. Res., 100, 24,691–24,703, https://doi.org/10.1029/95JC02554, 1995.

Maykut, G. A. and Untersteiner, N.: Some results from a time-dependent thermodynamic model of sea ice, J. Geophys. Res., 76, 1550–1575, https://doi.org/10.1029/JC076i006p01550, 1971.

McDougall, J. and Barker, P.: Getting started with TEOS-10 and the Gibbs Seawater (GSW) Oceanographic Toolbox, 28pp., SCOR/IAPSO WG127, ISBN 978-0-646-55621-5, 2011.

Menze, S., Ingvaldsen, R. B., Haugan, P., Fer, I., Sundfjord, A., Beszczynska-Moeller, A., and Falk-Petersen, S.: Atlantic Water Pathways Along the North-Western Svalbard Shelf Mapped Using Vessel-Mounted Current Profilers, Journal of Geophysical Research: Oceans, 124, 1699–1716, https://doi.org/10.1029/2018JC014299, 2019.

Meyer, A., Fer, I., Sundfjord, A., and Peterson, A. K.: Mixing rates and vertical heat fluxes north of Svalbard from Arctic winter to spring, J. Geophys. Res., 122, 4569–4586, https://doi.org/https://doi.org/10.1002/2016JC012441, 2017.

Musgrave, R. C., MacKinnon, J. A., Pinkel, R., Waterhouse, A. F., and Nash, J.: Tidally Driven Processes Leading to Near-Field Turbulence in a Channel at the Crest of the Mendocino Escarpment, J. Phys. Oceanogr., 46, 1137–1155, https://doi.org/10.1175/Jpo-D-15-0021.1, 2016.

Nash, J. D., Kunze, E., Lee, C. M., and Sanford, T. B.: Structure of the baroclinic tide generated at Kaena Ridge, Hawaii, Journal of Physical Oceanography, 36, 1123–1135, https://doi.org/10.1175/JPO2883.1, 2006.

Nasmyth, P.: Ocean turbulence, Ph.D. thesis, The University of British Columbia, 1970.

Oakey, N. S. and Elliott, A. J.: Dissipation within the surface mixed layer, J. Phys. Oceanogr., 12, 171–185, https://doi.org/10.1175/1520-0485(1982)012<0171:DWTSML>2.0.CO;2, 1982.

Osborn, T. R.: Estimates of the local rate of vertical diffusion from dissipation measurements, J. Phys. Oceanogr., 10, 83–89, 1980.

Padman, L. and Dillon, T. M.: Turbulent mixing near the Yermak Plateau during the coordinated Eastern Arctic Experiment, Journal of Geophysical Research: Oceans, 96, 4769–4782, https://doi.org/10.1029/90JC02260, 1991.

Padman, L. and Erofeeva, S.: A barotropic inverse tidal model for the Arctic Ocean, Geophysical Research Letters, 31, https://doi.org/10.1029/2003GL019003, 2004.

Padman, L., Plueddemann, A. J., Muench, R. D., and Pinkel, R.: Diurnal tides near the Yermak Plateau, J. Geophys. Res., 97, 12,639–12,652, https://doi.org/10.1029/92JC01097, 1992.

Peterson, A. K., Fer, I., McPhee, M. G., and Randelhoff, A.: Turbulent heat and momentum fluxes in the upper ocean under Arctic sea ice, Journal of Geophysical Research - Oceans, 122, 1–18, https://doi.org/10.1002/2016JC012283, 2017.

Polyakov, I. V., Pnyushkov, A. V., Alkire, M. B., Ashik, I. M., Baumann, T. M., Carmack, E. C., Goszczko, I., Guthrie, J., Ivanov, V. V., Kanzow, T., Krishfield, R., Kwok, R., Sundfjord, A., Morison, J., Rember, R., and Yulin, A.: Greater role for Atlantic inflows on sea-ice loss in the Eurasian Basin of the Arctic Ocean, Science, https://doi.org/10.1126/science.aai8204, 2017.

Polyakov, I. V., Padman, L., Lenn, Y. D., Pnyushkov, A., Rember, R., and Ivanov, V. V.: Eastern Arctic Ocean Diapycnal Heat Fluxes through Large Double-Diffusive Steps, J. Phys. Oceanogr., 49, 227–246, https://doi.org/10.1175/Jpo-D-18-0080.1, 2019.

Polyakov, I. V., Rippeth, T. P., Fer, I., Alkire, M. B., Baumann, T. M., Carmack, E. C., Ingvaldsen, R., Ivanov, V. V., Janout, M., Lind, S., et al.: Weakening of cold halocline layer exposes sea ice to oceanic heat in the eastern Arctic Ocean, Journal of Climate, https://doi.org/10.1175/JCLI-D-19-0976.1, 2020.

Rainville, L. and Winsor, P.: Mixing across the Arctic Ocean: Microstructure observations during the Beringia 2005 Expedition, Geophys. Res. Lett., 35, L08606, https://doi.org/10.1029/2008GL033532, 2008.

Rainville, L. and Woodgate, R. A.: Observations of internal wave generation in the seasonally ice-free Arctic, Geophys. Res. Lett., 36, L23604, https://doi.org/10.1029/2009GL041291, 2009.

Randelhoff, A., Fer, I., Sundfjord, A., Tremblay, J.-É., and Reigstad, M.: Vertical fluxes of nitrate in the seasonal nitracline of the Atlantic sector of the Arctic Ocean, Journal of Geophysical Research: Oceans, 121, 5282–5295, https://doi.org/10.1002/2016JC011779, 2016.

Randelhoff, A., Fer, I., and Sundfjord, A.: Turbulent upper-ocean mixing affected by meltwater layers during Arctic summer, Journal of Physical Oceanography, 47, 835–853, https://doi.org/10.1175/JPO-D-16-0200.1, 2017.

Rippeth, T. P., Lincoln, B. J., Lenn, Y.-D., Green, J. A. M., Sundfjord, A., and Bacon, S.: Tide-mediated warming of Arctic halocline by Atlantic heat fluxes over rough topography, Nature Geosci, 8, 191–194, https://doi.org/https://doi.org/10.1038/ngeo2350, 2015.

Rippeth, T. P., Vlasenko, V., Stashchuk, N., Scannell, B. D., Green, J. A. M., Lincoln, B. J., and Bacon, S.: Tidal Conversion and Mixing Poleward of the Critical Latitude (an Arctic Case Study), Geophys. Res. Lett., 44, 12 349–12 357, https://doi.org/10.1002/2017gl075310, 2017.

Rudels, B., Meyer, R., Fahrbach, E., Ivanov, V., Østerhus, S., Quadfasel, D., Schauer, U., Tverberg, V., and Woodgate, R.: Water mass distribution in Fram Strait and over the Yermak Plateau in summer 1997, Annales Geophysicae, 18, 687–705, https://doi.org/10.1007/s00585-000-0687-5, 2000.

Scheifele, B., Waterman, S., and Carpenter, J.: Turbulence and Mixing in the Arctic Ocean's Amundsen Gulf, J. Phys. Oceanogr., 2020.

Schmidtko, S., Johnson, G. C., and Lyman, J. M.: MIMOC: A global monthly isopycnal upper-ocean climatology with mixed layers, Journal of Geophysical Research: Oceans, 118, 1658–1672, https://doi.org/10.1002/jgrc.20122, 2013.

St. Laurent, L. C., Simmons, H. L., and Jayne, S. R.: Estimating tidally driven mixing in the deep ocean, Geophys. Res. Lett., 29, 2106, https://doi.org/10.1029/2002GL015633, 2002.

Timmermans, M.-L. and Marshall, J.: Understanding Arctic Ocean Circulation: A Review of Ocean Dynamics in a Changing Climate, Journal of Geophysical Research: Oceans, 125, https://doi.org/10.1029/2018JC014378, 2020.

Tsubouchi, T., Bacon, S., Aksenov, Y., Naveira Garabato, A. C., Beszczynska-Möller, A., Hansen, E., De Steur, L., Curry, B., and Lee, C. M.: The Arctic Ocean seasonal cycles of heat and freshwater fluxes: Observation-based inverse estimates, Journal of Physical Oceanography, 48, 2029–2055, https://doi.org/10.1175/JPO-D-17-0239.1, 2018.

Vlasenko, V., Stashchuk, N., Hutter, K., and Sabinin, K.: Nonlinear internal waves forced by tides near the critical latitude, Deep Sea Research Part I: Oceanographic Research Papers, 50, 317–338, https://doi.org/10.1016/S0967-0637(03)00018-9, 2003.

Våge, K., Pickart, R. S., Pavlov, V., Lin, P., Torres, D. J., Ingvaldsen, R., Sundfjord, A., and Proshutinsky, A.: The Atlantic Water boundary current in the Nansen Basin: Transport and mechanisms of lateral exchange, Journal of Geophysical Research: Oceans, 121, 6946–6960, https://doi.org/10.1002/2016JC011715, 2016.

Zhao, M., Timmermans, M.-L., Cole, S., Krishfield, R., Proshutinsky, A., and Toole, J.: Characterizing the eddy field in the Arctic Ocean halocline, J. Geophys. Res., 119, 8800–8817, https://doi.org/10.1002/2014jc010488, 2014.